



**HAL**  
open science

## Magneto-gravity-elliptic instability

Abdelaziz Salhi, Claude Cambon

► **To cite this version:**

Abdelaziz Salhi, Claude Cambon. Magneto-gravity-elliptic instability. *Journal of Fluid Mechanics*, 2023, 963, pp.A9. 10.1017/jfm.2023.300 . hal-04105868

**HAL Id: hal-04105868**

**<https://hal.science/hal-04105868v1>**

Submitted on 25 May 2023

**HAL** is a multi-disciplinary open access archive for the deposit and dissemination of scientific research documents, whether they are published or not. The documents may come from teaching and research institutions in France or abroad, or from public or private research centers.

L'archive ouverte pluridisciplinaire **HAL**, est destinée au dépôt et à la diffusion de documents scientifiques de niveau recherche, publiés ou non, émanant des établissements d'enseignement et de recherche français ou étrangers, des laboratoires publics ou privés.



Distributed under a Creative Commons Attribution 4.0 International License

Banner appropriate to article type will appear here in typeset article

# 1 Magneto-gravity-elliptic instability

2 **Abdelaziz Salhi<sup>1,2†</sup> and Claude Cambon<sup>2</sup>**

3 <sup>1</sup>Département de Physique, Faculté des Sciences de Tunis, Université Tunis El Manar, Tunis, Tunisia.

4 <sup>2</sup>Université de Lyon, Laboratoire de Mécanique des Fluides et d'Acoustique, UMR 5509, Ecole Centrale de  
5 Lyon, CNRS, UCBL, INSA F-69134 Ecully Cedex, France.

6 (Received xx; revised xx; accepted xx)

7 Magneto-gravity-elliptic instability is addressed here considering an unbounded strained  
8 vortex (with constant vorticity  $2\Omega$  and with ellipticity parameter  $\varepsilon$ ) of a perfectly conducting  
9 fluid subjected to a uniform axial magnetic field (with Alfvén velocity scaled from the basic  
10 magnetic field  $B$ ) and an axial stratification (with a constant Brunt-Väisälä frequency  $N$ ).  
11 Such a simple model allows us to formulate the stability problem as a system of equations  
12 for disturbances in terms of Lagrangian Fourier (or Kelvin) modes which is universal for  
13 wavelengths of the perturbation sufficiently small with respect to the scale of variation of  
14 the basic velocity gradients. It can model localised patches of elliptic streamlines which  
15 often appear in some astrophysical flows (stars, planets and accretion discs) that are tidally  
16 deformed through gravitational interaction with other bodies. In the limit case where the flow  
17 streamlines are exactly circular ( $\varepsilon = 0$ ), there are fast and slow magneto-inertia-gravity waves  
18 with frequencies  $\omega_{1,2}$  and  $\omega_{3,4}$ , respectively. Under the effect of finite ellipticity, the resonant  
19 cases of these waves,  $\omega_i - \omega_j = n\Omega$  ( $i \neq j$ ) ( $n$  being an integer), can become destabilising. The  
20 maximal growth rate of the subharmonic instability (related to the resonance of order  $n = 2$ )  
21 is determined by extending the asymptotic method by Lebovitz & Zweibel (*Astrophys. J.*, vol.  
22 609, 2004, pp. 301–312). The domains of the  $(k_0 B/\Omega, N/\Omega)$  plane for which this instability  
23 operates are identified ( $1/k_0$  being a characteristic length scale). We demonstrate that the  
24  $N \rightarrow 0$  limit is, in fact, singular (discontinuous). The axial stable stratification enhances the  
25 subharmonic instability related to the resonance between two slow modes because, at large  
26 magnetic field strengths, its maximal growth rate is twice that found in the case without  
27 stratification.

28 .

29 **Key words:** vortex instability, stratified astrophysical flows, MHD turbulence.

## 30 1. Introduction

31 The three-dimensional (3D) elliptical flow instability is very generic and occurs in many flow  
32 configurations, when the basic velocity field (or base flow) consists of large horizontal vortices  
33 with elliptical streamlines in their core. The elliptic instability is a parametric resonance of

† Email address for correspondence: lazizsalhi@yahoo.fr

34 internal (usually inertial) waves due to an elliptical deformation of the streamlines of a  
35 rotating flow. The reader is referred to Kerswell (2002) for a detailed review and references  
36 therein. The origin of the ellipticity in the core of eddies is multifold. In the study of the  
37 stability of airplane wakes, we have to consider the presence, before their possible breaking,  
38 of a pair of large counter-rotating vortices: this is the mutual induction of these eddies that  
39 render their core elliptic. More generally, the characteristics and behaviour of counter-rotating  
40 and corotating vortex pairs have been recently reviewed in the study by Leweke, Le Dizès &  
41 Williamson (2016).

42 In line with former studies, McKeown *et al.* (2020) showed that iterations of the elliptical  
43 instability, arising from the interactions between counter-rotating vortices, lead to the  
44 emergence of turbulence. As a second example, in rotating flows subjected to precession, the  
45 gyroscopic torque, mediated by the misalignment of solid-body rotation and system angular  
46 velocity, induces an additional shear that, superimposed to solid-body rotation, results in  
47 elliptical streamlines, as shown by Kerswell (1993a) and by Salhi & Cambon (2009) in the  
48 simplest geometry. More generally, elliptical shape caused by tidal forces is very common  
49 in many astrophysical systems such as planetary cores, binary stars, gaseous planets and  
50 accretion discs. The importance of elliptical instability, in a purely hydrodynamic context, in  
51 the tidal dissipation mechanism in such astrophysical systems has been the subject of several  
52 studies in the literature (Barker & Lithwick 2013; Cébron *et al.* 2013; Barker, Braviner  
53 & Ogilvie 2016; Barker 2016). Note that tidal dissipation generates heat in astrophysical  
54 systems, which in some cases may be important for their structure and evolution (Ogilvie  
55 2014).

56 Being the ellipticity due to the mutual induction of adjacent vortices or not, the elliptical  
57 instability is local, so that it is generally sufficient to consider a single elliptic eddy  
58 for the base (or mean) flow. For trailing vortices again, it has been shown that the  
59 Moore–Saffman–Tsai–Widnall (MSTW) instability (Moore & Saffman 1975; Tsai & Widnall  
60 1976), in the short-wavelength regime, is an elliptical instability (Éloy & Le Dizès 2001;  
61 Sipp & Jacquin 2003; Fukumoto 2003; Chang & Smith 2021). It is worth mentioning that  
62 the MSTW instability encompasses the long-wave instability bearing with Crow’s instability  
63 (Crow 1970) which occurs through the mutual induction of a pair of parallel counter-rotating  
64 vortex columns (McKeown *et al.* 2020): the Biot–Savart law is generally used to compute the  
65 induced velocity on one of the trailing vortices owing to the presence of the other. Recently,  
66 Feys & Maslowe (2016) have examined the elliptical instability of the Moore and Saffman  
67 model Moore & Saffman (1975) for a *single* trailing vortex. Their results demonstrate the  
68 significant effect of the distribution and intensity of the axial flow on the elliptical instability of  
69 a trailing vortex. Such a robust 3D instability leads to vortex decay under most circumstances,  
70 as reviewed by Lesur & Papaloizou (2009). Rather old experimental evidences are quoted in  
71 the following historical review, and recently the nonlinear fate of libration-induced elliptical  
72 instability in low-dissipation and low-forcing regimes has been explored experimentally by  
73 Le Reun, Favier & Le Bars (2019). They showed that once the saturation of the elliptical  
74 instability is reached, a turbulent state is observed for which the energy is injected only in  
75 the resonant inertial waves.

76 It is clear that the elliptical instability has a very long history, and deserves a survey, as  
77 follows. This allows us to discuss what is the simplest mathematical way to identify it and  
78 to quantify its effects, first in the neutral (non-stratified), purely hydrodynamical case. After  
79 some experimental evidences of that instability (Gledzer *et al.* 1975; Malkus 1989), see also  
80 the recent review by McKeown *et al.* (2020), a sudden interest arose when Pierrehumbert  
81 (1986) discovered its characteristic properties by a conventional normal mode analysis  
82 approach, whereas at the same time Bayly (1986) found the same results using the simpler  
83 and more elegant method using Kelvin modes, or mean-flow-advected (Lagrangian) Fourier

84 modes along elliptical trajectories. The latter study, similar to that by Craik & Criminale  
 85 (1986), was foreshadowed by a rapid distortion theory (RDT) analysis by Cambon (1982),  
 86 and Cambon *et al.* (1985) (in French). This is re-discussed, in English, by Godeferd,  
 87 Cambon & Leblanc (2001), with especially its figure 3, and in Sagaut & Cambon (2008,  
 88 2018) for a recent overview. Waleffe (1989, 1990) clearly described the physical mechanism  
 89 of the elliptical instability as a vortex stretching mechanism and showed how the growing  
 90 Kelvin modes found by Bayly (1986) in the case of unbounded strained vortex could be  
 91 superimposed to create a localised, unstable disturbance of the form found in the bounded  
 92 elliptical cylinder case (Gledzer *et al.* 1975).

93 From the previous studies, let us summarise the advantages of the formalism with  
 94 projection of the disturbance fields onto Kelvin modes. The Kelvin modes are essentially  
 95 3D Fourier modes, even if the wave vector can become time-dependent following the  
 96 mean flow streamlines. The time dependency of the wave vector represents the convection  
 97 of the plane wave  $\exp(i\mathbf{k}(t)\cdot\mathbf{x})$  by the base flow. Both the direction and magnitude of  
 98  $\mathbf{k}$  change as wave crests rotate and approach or separate from each other due to basic  
 99 velocity gradients. Accordingly, all the formal advantages of Fourier space remain valid:  
 100 pure algebraic formulation of integro-differential equations, including Poisson equation for  
 101 pressure disturbances, algebraic dissipation term instead of Laplacian operator, algebraic  
 102 linkage from vorticity to velocity (instead of a Biot-Savart relationship). It is worth  
 103 emphasising that the system of equations for disturbances in terms of Lagrangian Fourier  
 104 modes is universal under a typical length scale. Indeed, such a system is recovered for small-  
 105 scale disturbances traveling near any smooth base-flow trajectory, in the zonal asymptotic  
 106 method of Lifschitz & Hameiri (1991) with close connection with geometric optics; the  
 107 velocity gradients of the base flow are treated as space-uniform in a domain of unspecified  
 108 length scale, asymptotically small (see also Godeferd, Cambon & Leblanc (2001)).

109 Can the elliptic instability, in the pure hydrodynamic context, survive in the presence  
 110 of vertical basic density stratification, that is stabilising considered alone? A first answer  
 111 is given by the study of the stability of inertia-gravity waves when it is altered by the  
 112 ellipticity of streamlines. In relation to the dynamics of ocean and atmosphere Miyazaki &  
 113 Fukumoto (1992); Miyazaki (1993) investigated the influence of the Coriolis force and  
 114 density stratification, caused by temperature or salinity gradient, on the elliptical instability.  
 115 Miyazaki & Fukumoto (1992) considered an unbounded strained-vortex flow with stable  
 116 axial stratification. They have found that the growth rates for the elliptical instability were  
 117 invariably reduced: the subharmonic elliptical instability is completely suppressed when  
 118 Brunt-Väisälä frequency ( $N$ ) is greater or equal to the half of the basic vorticity strength ( $\Omega$ ).  
 119 For small eccentricities, asymptotic theory leads to formulae for the maximum growth rate  
 120 (Kerswell 2002) (see also § 3 in the present study). It is worth mentioning that the elliptical  
 121 instability of stratified vortices has been addressed as well in previous studies (Otheguy,  
 122 Chomaz & Billant 2006; Le Bars & Le Dizès 2006; Guimbard *et al.* 2010; Suzuki, Hirota  
 123 & Hattori 2018). The effects of differential diffusion between momentum and density on the  
 124 elliptical instability have recently been addressed by Singh & Mathur (2019). They showed  
 125 that, in the case where the ratio of thermal diffusivity to kinematic diffusivity is equal to  
 126 unity, the viscous effects are purely suppressive, whereas for sufficiently small values of this  
 127 ratio, there is an oscillatory instability whose signature is nevertheless present with zero  
 128 growth rate in the inviscid limit. In turbulent Rayleigh-Bénard convection, Zwirner, Tilgner  
 129 and Shishkina (2020) showed that the mechanism which causes the twisting and breaking of  
 130 a single-roll large-scale circulation into multiple rolls is the elliptical instability. On the other  
 131 hand, density effects on the MSTW instability have been recently investigated by Chang &  
 132 Smith (2021) who performed a normal mode stability analysis and showed that, for the

133 subharmonic instability (resonance  $(m, m + 2) = (0, 2)$ ,  $m$  being the azimuthal wavenumber)  
134 the growth rate is maximised when the ratio of vortex to ambient fluid density is near 0.215.

135 The interaction of vortices with a magnetic field is a fundamental process in astrophysical  
136 magnetohydrodynamics (MHD). Therefore, a similar question occurs when one moves from  
137 hydrodynamics to MHD when the electrically conducting elliptical flow is subjected to an  
138 unperturbed (or a basic) magnetic field. In a geophysical context, Kerswell (1994) studied the  
139 effect of a toroidal magnetic field on the elliptic instability in a rotating spheroidal container  
140 filled with an incompressible electrically conducting fluid, which carries a constant axial  
141 electric current. He concluded that the toroidal magnetic field has a stabilizing influence. By  
142 including the effect of a uniform magnetic field perpendicular to the plane of the elliptical base  
143 flow, the resulting magneto-elliptic instability has been related to the problem of turbulence  
144 generation and, hence, momentum transport in accretion discs by Lebovitz & Zweibel  
145 (2004) (hereafter LZ04). In that study, an analytical technique was developed to determine  
146 the maximal growth rates of the destabilising resonances of order  $n = 2$  (i.e., subharmonic  
147 instabilities, see equation (1.1)) in the limit of small elliptical (tidal) deformations. This  
148 analytical technique has been used in previous studies by Mizerski & Bajer (2009) for the  
149 magneto-elliptical instability of rotating systems and by Salhi, Lehner & Cambon (2010)  
150 for the magneto-precessional instability. Herreman *et al.* (2010) conducted experiments to  
151 explain some aspects of the nonlinear transition process for the elliptic instability in rotating  
152 cylinders under imposed magnetic field. It is worth noting that in the case where the Coriolis  
153 and Lorentz forces are simultaneously present and when the wave vector  $\mathbf{k}$  aligns with the  
154 magnetic field the elliptical flow can develop horizontal instability which dominates over  
155 all other modes (Bajer & Mizerski 2013). In the astrophysical context (tidal dissipation in  
156 gaseous planets and stars), Barker & Lithwick (2014) found that magnetic fields do prevent  
157 vortices from forming and, hence, greatly enhance the steady-state dissipation rate.

158 The combined effects of stable density stratification and MHD on the elliptical instability  
159 within an elliptically distorted cylinder have been investigated by Kerswell (1993b).  
160 He performed a normal mode stability analysis for a simple configuration possessing  
161 considerable symmetry between the velocity and magnetic fields: a purely azimuthal  
162 magnetic field, which in the frozen flux limit is also elliptically distorted. In that study,  
163 stratification is either axial (the isopycnics are parallel to the streamlines) or radial (the  
164 isopycnics are perpendicular to the streamlines).

165 In the present paper we analyse in detail the joint influence of a stable axial stratification  
166 (with strength  $N$ ) and an external (axial) uniform magnetic field (with Alfvén velocity  
167 scaled from the basic magnetic field  $B$ ) on the stability of an unbounded flow with elliptical  
168 streamlines of a perfectly conducting fluid. Our study extends the study by Miyazaki &  
169 Fukumoto (1992) by including the effects of a magnetic field and also the study by LZ04  
170 by including the effects of an axial stable stratification. An important aspect of the present  
171 study is to map out the regime of  $(B/(L_0\Omega), N/\Omega)$  space ( $L_0$  being a characteristic length  
172 scale) for which the destabilising resonances of order  $n = 2$  (see equation (1.1)) of magneto-  
173 inertia-gravity (MIG) waves prone to operate and to determine their growth rates at small  
174 ellipticity by extending the analytical technique by LZ04. In the laboratory experiment of  
175 a magnetised turbulent Taylor-Couette flow of liquid metal by Nornberg *et al.* (2010),  
176 the combined fast and slow Alfvén-inertial waves were clearly identified where the observed  
177 slow wave is damped. These authors have identified a relationship between the slow magneto-  
178 inertial waves and the magneto-rotational instability (MRI) (Balbus & Hawley 1991; Wang  
179 *et al.* 2022). On the other hand, Mizerski & Lyra (2012) examined the link between the  
180 magneto-elliptical instability and the MRI, explaining that the two instabilities are different  
181 manifestations of the same magneto-elliptical-rotational instability. Salhi *et al.* (2012) have  
182 studied the effects of stable stratification on the MRI instability and showed that, under the

183 MHD Boussinesq approximation (e.g. Wilczyński, Hughes & Kersalé (2022)), the so-called  
 184 “magnetic induction potential scalar” (MIPS, i.e., the scalar product of the magnetic field  
 185 vector and the density gradient) is a Lagrangian invariant for a non-diffusive fluid. In contrast,  
 186 the potential vorticity (PV), which is very useful as an invariant in stratified geophysical flows  
 187 (e.g. Pedlow (2013)), is no longer valid in MHD because it removes the baroclinic torque  
 188 in the extended vorticity equation, but not the counterpart of the Lorentz force.

189 An asymptotic stability analysis is developed in section 3 at leading order in the ellipticity  
 190 parameter  $\varepsilon$  in order to determine the growth rates of the (subharmonic) instability tongues  
 191 that emanate from the points at vanishing ellipticity. In this limit, disturbances to the basic  
 192 flow are found in terms of MIG dispersive waves, with a dispersion law (Salhi *et al.* 2017)  
 193 that includes  $\Omega$ ,  $N$ ,  $B/L_0$  and the angular parameter  $\mu = \cos(\theta)$  (the angle  $\theta$  being the  
 194 angle between the wave vector of the perturbations and that of the base-flow vorticity). In  
 195 contrast with particular cases, the general dispersion law of MIG waves is no longer a simple  
 196 combination of the individual dispersion frequencies, considered alone, but is obtained in  
 197 combining the eigenvalues of the matrix of the whole linear system of equations (Salhi *et al.*  
 198 *et al.* 2017). Fast and slow modes are identified, with different resonance conditions between  
 199 them, or

$$200 \quad \omega_i - \omega_j = n\Omega \quad (i, j = 1, 2, 3, 4, i \neq j, n \text{ being an integer}). \quad (1.1)$$

201 Without an analysis of the resonant conditions, it is not possible to simply identify the different  
 202 instabilities, namely if they are subharmonic or not, if they result from the interaction of two  
 203 fast modes, two slow modes, or one fast and one slow.

204 As detailed in section 2, the use of the *magnetic invariant* (MIPS) makes it possible  
 205 to reduce the linear system of ordinary differential equations, which represents a Floquet  
 206 problem, from a five-component system to a four-component system only. In §3, we show  
 207 that stable stratification enhances the destabilising resonance of order  $n = 2$  between two  
 208 slow modes because we find that, at large magnetic strengths, its growth rate is about twice  
 209 that found in the case without stratification (LZ04). Asymptotic formulae are compared with  
 210 numerical results carried out at arbitrary ellipticity in Section 4. The effect of diffusion is  
 211 briefly addressed in the special case where the diffusion coefficients (kinetic, thermal and  
 212 magnetic) are equal. Conclusions and perspectives are offered in Section 5.

## 213 2. MHD Boussinesq’s equations

214 We consider a stratified electrically conducting fluid. Density variations are introduced using  
 215 the Boussinesq approximation for simplicity (Chandrasekhar 1961). The fluid is assumed to  
 216 be inviscid and non-diffusive. The effect of viscosity ( $\nu$ ) and thermal ( $\kappa$ ) and magnetic ( $\eta$ )  
 217 diffusivity are briefly addressed in §4.3 by considering the case where  $\nu = \kappa = \eta$  (i.e., the  
 218 case where the magnetic and thermal Prandtl numbers are unity)

219 The Boussinesq MHD equations written in a fixed frame take the form (Davidson 2013)

$$220 \quad D_t \tilde{\mathbf{u}} = -\nabla \tilde{p} + \left( \tilde{\mathbf{b}} \cdot \nabla \right) \tilde{\mathbf{b}} + \tilde{\vartheta} \mathbf{n} + \nu \nabla^2 \tilde{\mathbf{u}}, \quad (2.1a)$$

$$221 \quad D_t \tilde{\mathbf{b}} = \left( \tilde{\mathbf{b}} \cdot \nabla \right) \tilde{\mathbf{u}} + \eta \nabla^2 \tilde{\mathbf{b}}, \quad (2.1b)$$

$$222 \quad D_t \tilde{\vartheta} = \kappa \nabla^2 \tilde{\vartheta} \quad (2.1c)$$

$$223 \quad \nabla \cdot \tilde{\mathbf{u}} = 0 \quad (2.1d)$$

$$224 \quad \nabla \cdot \tilde{\mathbf{b}} = 0 \quad (2.1e)$$

226 where  $D_t(\cdot) \equiv (\partial_t + \tilde{\mathbf{u}} \cdot \nabla)(\cdot)$  denotes the material derivative,  $\tilde{\mathbf{u}}$  denotes the velocity and  $\tilde{\mathbf{b}}$

227 denotes the magnetic field which is scaled using Alfvén velocity units, i.e., it is divided by  
 228  $\sqrt{\rho_0\mu_0}$  where  $\rho_0$  and  $\mu_0$  are the constant density and the magnetic permeability of the fluid.  
 229 Here,  $\tilde{p}$  being the total pressure (including the magnetic part) divided by the constant density  
 230  $\rho_0$ . In the present study, we consider axial stratification,

$$231 \quad \mathbf{n} = \mathbf{e}_3 = -\mathbf{g}/g. \quad (2.2)$$

232 where  $\mathbf{e}_3$  is the upward vertical unit vector and  $\mathbf{g}$  is the gravitational acceleration vector. The  
 233 first equation in the above system is the momentum equation, the second is the induction  
 234 equation for the magnetic field and the third is the buoyancy scalar equation. Both velocity  
 235 field and magnetic field are solenoidal (Eq. (2.1-d,e)).

236 For a non magnetised Boussinesq ideal fluid, one may easily show that the potential  
 237 vorticity (PV) (Pedlowsky 2013),

$$238 \quad \tilde{\omega}_\kappa = \tilde{\omega}_a \cdot \nabla \tilde{\vartheta}, \quad (2.3)$$

239 is a Lagrangian, invariant, i.e.,  $D_t \tilde{\omega}_\kappa = 0$ . Here,  $\tilde{\omega}_a$  is the absolute vorticity vector which,  
 240 in the absence of the Coriolis force, identifies with the vorticity vector  $\mathbf{W} = \nabla \times \tilde{\mathbf{u}}$ . In  
 241 counterpart, for a magnetised Boussinesq ideal fluid, it is the so-called MIPS (Salhi *et al.*  
 242 2012)

$$243 \quad \tilde{\omega}_m = \tilde{\mathbf{b}} \cdot \nabla \tilde{\vartheta} \quad (2.4)$$

244 that is a Lagrangian invariant, i.e.,  $D_t \tilde{\omega}_m = 0$ , and not  $\tilde{\omega}_\kappa$ . The usefulness of introducing  
 245 the MIPS is illustrated later.

### 246 2.1. Base flow

247 The solutions of system (2.1) are conveniently decomposed into a 'basic flow' ( $\mathbf{U}, P, \mathbf{B}, \Theta$ )  
 248 and a 'disturbance' ( $\mathbf{u}, p, \mathbf{b}, \vartheta$ ), but the latter needs to be small compared with the former,

$$249 \quad \tilde{\mathbf{u}} = \mathbf{U} + \mathbf{u}, \quad \tilde{p} = P + p, \quad \tilde{\mathbf{b}} = \mathbf{B} + \mathbf{b}, \quad \tilde{\vartheta} = \Theta + \vartheta. \quad (2.5)$$

250 We consider the linear stability of a stratified vortical flow with elliptical streamlines and  
 251 with uniform vertical magnetic field (see figure 1)

$$252 \quad \mathbf{U} = \mathbf{A} \cdot \mathbf{x}, \quad \mathbf{A} = \Omega \begin{pmatrix} 0 & -E & 0 \\ E^{-1} & 0 & 0 \\ 0 & 0 & 0 \end{pmatrix} \quad (2.6a)$$

$$253 \quad \mathbf{B} = B \mathbf{e}_3, \quad (2.6b)$$

$$254 \quad \Theta = N^2 x_3 \quad (2.6c)$$

256 where  $\Omega$  is a constant that is a measure of the intensity of the flow and  $E \geq 1$  is a measure  
 257 of elliptical deformation of the streamlines, and  $N$  is the Brunt-Väisälä frequency such that

$$258 \quad N^2 = -\frac{g}{\rho_0} \frac{d\rho}{dx_3}. \quad (2.7)$$

259 Circular streamlines correspond to the case where  $E = 1$ . The parameter

$$260 \quad \varepsilon = \frac{1}{2} (E - E^{-1}) \quad (2.8)$$

represents the departure of the streamlines of the unperturbed flow from axial symmetry. We  
 note that

$$0 < \delta = (E - E^{-1}) / (E + E^{-1}) < 1$$

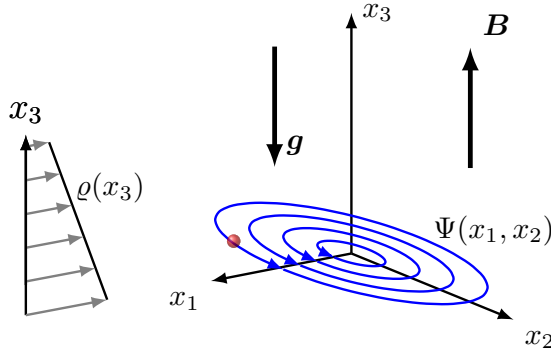


Figure 1

A schematic drawing of the basic state – planar flow with elliptical streamlines,  $\Psi = -(\Omega/2) (E^{-1}x_1^2 + Ex_2^2)$  being the stream function in the presence of an axial uniform magnetic field ( $\mathbf{B} = B\mathbf{e}_3$ ) and an axial stable stratification ( $\Theta = N^2x_3$ ,  $N^2 = -(g/\rho_0)(d\rho/dx_3)$ ,  $N$  being the Brunt-Väisälä frequency). The gravity vector is given by  $\mathbf{g} = -g\mathbf{e}_3$  with  $g > 0$ .

261 for the flow to be elliptical. We also note that, an equivalent form for the unperturbed velocity  
 262 field has been used in previous studies (Waleffe 1990; Miyazaki & Fukumoto 1992; Miyazaki  
 263 1993; Kerswell 2002; Mizerski & Bajer 2009; Bajer & Mizerski 2013)

$$264 \quad \mathbf{U} = \Gamma [-(1 + \delta)x_2\mathbf{e}_1 + (1 - \delta)x_1\mathbf{e}_2], \quad (2.9)$$

265 where  $2\Gamma = \Omega(E + E^{-1})$  and  $-\Gamma\delta$  represents the strain rate, but the expression (2.6a) seems  
 266 more suitable for analysing resonant destabilisation (Mizerski & Bajer 2009).

267 The basic buoyancy scalar  $\Theta$  varies linearly with the axial coordinate  $x_3$  (axial stratification)  
 268 and is proportional to the gravitational acceleration,  $g$ , and to a background density  
 269 (or temperature) gradient. This linear profile admits a constant Brunt-Väisälä frequency  
 270  $N$  throughout the entire fluid. More general exact solutions of the combined stratified  
 271 fluid/magnetic equations exist in an unbounded domain (Craig 1989); the case in hand  
 272 (i.e. equation (2.6)) is probably the simplest of these. As indicated previously, Miyazaki &  
 273 Fukumoto (1992) considered an unbounded strained-vortex flow with stable exponential  
 274 stratification in the axial direction at small Froude number,  $\text{Fr} = \Gamma^2 L_0/g \ll 1$  with  $L_0$   
 275 a characteristic length scale. One may show that the resulting linear differential system for the  
 276 disturbances superimposed on the base flow is the same considering either an exponential  
 277 basic stratification or a linear (with respect to space coordinates) basic stratification. Both  
 278 profiles (exponential or linear) admit a constant Brunt-Väisälä frequency through-out the  
 279 entire fluid.

280

## 2.2. Perturbed system

281 In the following, we consider the case of a non-diffusive fluid. Diffusivity effects with the  
 282 assumption that the diffusion coefficients are equal ( $\nu = \kappa = \eta$ ) or, equivalently, the magnetic  
 283 and thermal Prandtl numbers are equal to one are briefly discussed at the end of §4.

### 284 2.2.1. Linearized system in physical space

285 We substitute the solutions (2.5) into the system (2.1) and linearise. Linearisation is not  
 286 readily justified by the fact that the flow disturbances are very small with respect to the base  
 287 flow. Linearisation is briefly discussed in the conclusion. Thus, we expect our analysis to



288 break down when the disturbances become so large that nonlinear effects become important.  
 289 The resulting perturbed equations are

$$290 \quad D_t \mathbf{u} = -\nabla p - (\mathbf{u} \cdot \nabla) \mathbf{U} + (\mathbf{B} \cdot \nabla) \mathbf{b} + \vartheta \mathbf{e}_3, \quad (2.10a)$$

$$291 \quad D_t \mathbf{b} = (\mathbf{b} \cdot \nabla) \mathbf{U} + (\mathbf{B} \cdot \nabla) \mathbf{u}, \quad (2.10b)$$

$$292 \quad D_t \vartheta = -N^2 u_3, \quad (2.10c)$$

$$293 \quad \nabla \cdot \mathbf{u} = 0, \quad (2.10d)$$

$$294 \quad \nabla \cdot \mathbf{b} = 0. \quad (2.10e)$$

296 As for the linear part of MIPS (see Eq. (2.4)), it takes the form

$$297 \quad \varpi_m = B \frac{\partial \vartheta}{\partial x_3} + N^2 b_3. \quad (2.11)$$

298 where  $D_t \varpi_m = 0$ , so that  $\varpi_m = \text{constant}$ . As shown later, for the purposes of studying  
 299 stability, we may set  $\varpi_m = 0$  (see also Benkacem *et al.* (2022)).

### 300 2.2.2. Floquet system in wave space.

301 The disturbances are expressed in terms of Lagrangian Fourier modes, as discussed in section  
 302 1. These modes were used for shear waves by Moffatt (2010), who was probably the first to  
 303 call them ‘Kelvin modes’, in reference to a pioneering paper by Lord Kelvin Kelvin (1887)  
 304 in the nineteenth century. They are advected by the mean flow as Lagrangian invariants  
 305 (Cambon 1982; Sagaut & Cambon 2008, 2018), as plane waves for which the direction and  
 306 the speed of propagation depend on time, via a time-dependent wave vector:

$$307 \quad [\mathbf{u}, p, \mathbf{b}, \vartheta] (\mathbf{x}, t) = [\hat{\mathbf{u}}, \hat{p}, \hat{\mathbf{b}}, \hat{\vartheta}] (\mathbf{k}, t) \exp(\mathbf{i}\mathbf{x} \cdot \mathbf{k}(t)), \quad (2.12)$$

where  $i^2 = -1$ . Accordingly, the material derivative of the fluctuating velocity can be  
 rewritten as

$$D_t \mathbf{u} = \left( \partial_t + U_j \frac{\partial}{\partial x_j} \right) [\hat{\mathbf{u}}(\mathbf{k}, t) \exp(\mathbf{i}\mathbf{x} \cdot \mathbf{k}(t))]$$

with  $U_j = A_{jm} x_m$ , so that

$$D_t \mathbf{u} = [\partial_t \hat{\mathbf{u}} + \mathbf{i} ((d_t k_j) x_j + A_{jm} k_j x_m) \hat{\mathbf{u}}] \exp(\mathbf{i}\mathbf{x} \cdot \mathbf{k}(t)),$$

or, equivalently,

$$D_t \mathbf{u} = \left( \partial_t \hat{\mathbf{u}} + \mathbf{i} \left[ (d_t \mathbf{k} + A^T \mathbf{k}) \cdot \mathbf{x} \right] \hat{\mathbf{u}} \right) \exp(\mathbf{i}\mathbf{x} \cdot \mathbf{k}(t)).$$

308 In order to remove the explicit dependence on  $\mathbf{x}$  in the resulting equations for the Fourier  
 309 amplitudes  $\hat{\mathbf{u}}$ ,  $\hat{\mathbf{b}}$ ,  $\hat{p}$  and  $\hat{\vartheta}$ , one has to ensure that  $\mathbf{k}(t)$  varies in time according to the eikonal  
 310 equation

$$311 \quad d_t \mathbf{k} = -\mathbf{A}^T \cdot \mathbf{k}, \quad (2.13)$$

312 where  $d_t(\cdot) \equiv d(\cdot)/dt$  and  $T$  denotes transpose. Equation (2.13) can be solved to give

$$313 \quad k_1 = k_p \cos(\tau - \phi), \quad k_2 = E k_p \sin(\tau - \phi), \quad k_3 = k_{30}, \quad (2.14)$$

where  $\tau = \Omega t$  being a dimensionless time,

$$k_p^2 = k_1^2 + E^{-2} k_2^2 = k_{10}^2 + E^{-2} k_{20}^2, \quad \tan \phi = -E^{-1} k_{20}/k_{10},$$

314 with  $k_{j0}$  ( $j = 1, 2, 3$ ) the initial wave vector component. For purposes of studying stability,  
 315 we may set  $\phi = 0$ . This is easily seen by making the substitution  $\Omega t' = \Omega t + \phi$ , which  
 316 eliminates  $\phi$  from the equation.

317 Substituting the plane waves solution (2.12) into the system (2.10) and taking into account  
318 the eikonal equation (2.13), we obtain

$$319 \quad d_t \hat{\mathbf{u}} = -i\hat{p}\mathbf{k} - \mathbf{A}\cdot\hat{\mathbf{u}} + i(k_3 B)\hat{\mathbf{b}} + \hat{\vartheta}\mathbf{e}_3, \quad (2.15a)$$

$$320 \quad d_t \hat{\mathbf{b}} = \mathbf{A}\cdot\hat{\mathbf{b}} + i(k_3 B)\hat{\mathbf{u}}, \quad (2.15b)$$

$$321 \quad d_t \hat{\vartheta} = -N^2 \hat{u}_3, \quad (2.15c)$$

322 together with  $\mathbf{k}\cdot\hat{\mathbf{u}} = 0$  and  $\mathbf{k}\cdot\hat{\mathbf{b}} = 0$ . The use of the latter conditions allows one to eliminate  
324 the Fourier amplitude of fluctuating pressure,

$$325 \quad \hat{p}(\mathbf{k}, t) = -ik^{-2} \left( 2\Omega^2 \hat{c}_1 + k_3 \hat{\vartheta} \right), \quad \Omega \hat{c}_1 = Ek_1 \hat{u}_2 - E^{-1} k_2 \hat{u}_1, \quad (2.16)$$

326 and to reduce the above seven-component Floquet system to a five-component version. Here,  
327  $k = \sqrt{k_1^2 + k_2^2 + k_3^2}$  is the modulus of the wave vector. This reduction of components results  
328 from the fact that both Fourier modes for fluctuating velocity and for fluctuating magnetic  
329 field are two-component in the plane normal to the wave vector. Such projection can be done  
330 using the orthonormal Craya-Herring frame of reference, as used in several articles (e.g.  
331 from Salhi & Cambon (1997)).

332 We note that the case where the wave vector is vertical, so that  $k_1 = k_2 = 0$ ,  $k_p = 0$   
333 and  $k_3 = \pm k$ , characterises a special class of disturbances, called horizontal perturbations,  
334 in which the vertical components  $\hat{u}_3$  and  $\hat{b}_3$  identically vanish (Bajer & Mizerski 2013). In  
335 that case, axial stratification has no effect on the horizontal perturbations, and then there is  
336 no instability without the Coriolis force.

### 337 2.2.3. Change of variables

338 At  $k_3 = 0$ , the solution of the resulting Floquet system (2.15) is stable. Accordingly, we  
339 henceforth consider only perturbations with vertical wave number  $k_3 \neq 0$ . As in the studies  
340 by LZ04 and by Mizerski & Bajer (2009), we transform the resulting Floquet system in  
341 terms of the following variables to facilitate subsequent calculations

$$342 \quad \Omega \hat{c}_2 = -k_3 \hat{u}_3, \quad \Omega \hat{c}_3 = Ek_1 \hat{b}_2 - E^{-1} k_2 \hat{b}_1, \quad \Omega \hat{c}_4 = -k_3 \hat{b}_3, \quad \Omega^2 \hat{c}_5 = -k_3 \hat{\vartheta}. \quad (2.17)$$

343 Given (2.16) we transform the system (2.15) according to these new variables,

$$344 \quad d_\tau \hat{c}_1 = -4\varepsilon \frac{k_1 k_2}{k^2} \hat{c}_1 - 2\hat{c}_2 + i \frac{(k_3 B)}{\Omega} \hat{c}_3 + 2\varepsilon \frac{k_1 k_2}{k^2} \hat{c}_5 \quad (2.18a)$$

$$345 \quad d_\tau \hat{c}_2 = 2 \frac{k_3^2}{k^2} \hat{c}_1 + i \frac{(k_3 B)}{\Omega} \hat{c}_4 + \frac{k_1^2}{k^2} \hat{c}_5 \quad (2.18b)$$

$$346 \quad d_\tau \hat{c}_3 = i \frac{(k_3 B)}{\Omega} \hat{c}_1 \quad (2.18c)$$

$$347 \quad d_\tau \hat{c}_4 = i \frac{(k_3 B)}{\Omega} \hat{c}_2 \quad (2.18d)$$

$$348 \quad d_\tau \hat{c}_5 = -\frac{N^2}{\Omega^2} \hat{c}_2 \quad (2.18e)$$

350 where  $d_\tau \hat{c}_1 = \Omega^{-1} d_t \hat{c}_1$  and  $k_\perp = \sqrt{k_1^2 + k_2^2}$ . Combining equations (2.18d) and (2.18e), we  
351 deduce the following relation:

$$352 \quad -\frac{\Omega}{k_3} \left[ i\Omega (k_3 B) \hat{c}_5 + N^2 \hat{c}_4 \right] = i (k_3 B) \hat{\vartheta} + N^2 \hat{b}_3 = \hat{\omega}_m = \text{constant} \quad (2.19)$$

353 which represents the spectral counterpart of the MIPS (see Eq. (2.4)). Accordingly, system  
354 (2.18) can be further reduced to a fourth-order inhomogeneous Floquet system,

$$355 \quad d_\tau \hat{\mathbf{c}} = \mathbf{D}(\tau) \cdot \hat{\mathbf{c}} + \hat{\boldsymbol{\varphi}} \quad (2.20)$$

356 where the only non-zero elements of  $\mathbf{D}(\tau)$  are

$$357 \quad D_{11} = -4\varepsilon \frac{k_1 k_2}{k^2}, \quad D_{12} = -2, \quad D_{21} = 2 \frac{k_3^2}{k^2}, \quad (2.21a)$$

$$358 \quad D_{13} = D_{31} = D_{42} = i \frac{(k_3 B)}{\Omega}, \quad (2.21b)$$

$$359 \quad D_{14} = 2i\varepsilon \frac{N^2}{\Omega(k_3 B)} \frac{k_1 k_2}{k^2}, \quad (2.21c)$$

$$360 \quad D_{24} = i \left( \frac{(k_3 B)}{\Omega} + \frac{N^2}{\Omega(k_3 B)} \frac{k_\perp^2}{k^2} \right). \quad (2.21d)$$

362 The non-zero components of the inhomogeneous term in Eq. (2.20) take the form

$$363 \quad \hat{\varphi}_1 = 2i\varepsilon \frac{k_1 k_2}{k^2} \frac{\hat{\omega}_m}{(\Omega^2 B)}, \quad (2.22a)$$

$$364 \quad \hat{\varphi}_2 = i \frac{k_\perp^2}{k^2} \frac{\hat{\omega}_m}{(\Omega^2 B)} \quad (2.22b)$$

366 and it can be seen as a time-varying forcing excitation.

367 Note that in the non-magnetised stratified case, one can use the fact that the PV is  
368 a Lagrangian invariant for a non-diffusive fluid (Pedlow 2013) to derive a non-  
369 homogeneous two-component Floquet system in terms of the variables  $\hat{c}_1$  and  $\hat{c}_2$ .

### 2.3. Homogeneous Floquet system

371 The linear system (2.20) has the properties  $\mathbf{D}(\tau + T) = \mathbf{D}(\tau)$  and  $\hat{\boldsymbol{\varphi}}(\tau + T) = \hat{\boldsymbol{\varphi}}(\tau)$  where  
372  $T = 2\pi$  is the period common to both the matrix  $\mathbf{D}$  and the vector  $\hat{\boldsymbol{\varphi}}$ . Floquet theory does not  
373 address stability of the inhomogeneous system described by Eq. (2.20) where the 'forcing  
374 excitation'  $\hat{\boldsymbol{\varphi}}(\tau)$  is present. However, the  $T$ -periodic nature of  $\hat{\boldsymbol{\varphi}}(\tau)$  allows an extension to  
375 the theory (Slane & Tragesser 2011). Following the study of Slane & Tragesser (2011), it  
376 is shown that the basic behaviour of the homogeneous system

$$377 \quad d_\tau \hat{\mathbf{c}} = \mathbf{D} \cdot \hat{\mathbf{c}} \quad (2.23)$$

378 does not change with the addition of the term  $\hat{\boldsymbol{\varphi}}(\tau)$ . Here,  $\hat{\mathbf{c}} = (\hat{c}_1, \hat{c}_2, \hat{c}_3, \hat{c}_4)^T$  in the  
379 canonical basis of  $\mathbb{C}^4$ . In other words, for purposes of studying stability, one may set  $\hat{\omega}_\kappa = 0$ ,  
380 so that  $\hat{\boldsymbol{\varphi}} = \mathbf{0}$  (Benkacem *et al.* 2022).

381 We denote by  $\boldsymbol{\Phi}(\tau)$  any fundamental matrix solution of the homogeneous system (2.23)  
382 where  $\boldsymbol{\Phi}(0) = \mathbf{I}_4$ . According to Floquet–Lyapunov theorem,  $\boldsymbol{\Phi}$  is expressible in the form  
383 (Kuchment 1993),

$$384 \quad \boldsymbol{\Phi}(\tau) = \mathbf{F}(\tau) \exp(\mathbf{K}\tau), \quad (2.24)$$

385 where  $\mathbf{F}(\tau)$  is a non-singular continuous  $2\pi$ -periodic  $4 \times 4$  matrix-function (whose derivative  
386 is an integrable piecewise-continuous function) and  $\mathbf{K}$  is a constant matrix. The determinant  
387 of  $\boldsymbol{\Phi}$  is unity at  $\tau = 2\pi$ ,  $|\boldsymbol{\Phi}(2\pi)| = 1$  because

$$388 \quad \text{trace } \mathbf{D} = \sum_{j=1}^4 D_{jj} = -4\varepsilon \frac{k_1 k_2}{k^2} = -\frac{1}{k^2} d_\tau k^2. \quad (2.25)$$

389 It follows that whenever  $\lambda$  is an eigenvalue of the monodromy matrix,  $\mathbf{M} = \Phi(2\pi)$ , so too  
 390 are its inverse  $\lambda^{-1}$  and its complex conjugate  $\lambda^*$  (see LZ04). Consequently, in the stable case,  
 391 eigenvalues of  $\mathbf{M}$  lie on the unit circle. If any eigenvalue  $\lambda$  of  $\mathbf{M}$  has modulus exceeding one,  
 392 this implies that there is indeed an exponentially growing solution. The growth rates are then  
 393 given by

$$394 \quad \sigma = \frac{1}{2\pi} \log(\lambda). \quad (2.26)$$

395 In the Floquet system (2.23) figure four dimensionless parameters, namely

$$396 \quad \varepsilon = \frac{1}{2} (E - E^{-1}), \quad \mu = k_3/k_0, \quad \mathcal{N} = N/\Omega, \quad \mathcal{B} = (k_0 B)/\Omega \quad (2.27)$$

397 where  $k_0 = \sqrt{k_p^2 + k_3^2}$  represents the modulus of the initial wave vector for  $\varepsilon = 0$ . The  
 398 parameters  $k_0 B$ ,  $N$  and  $2\Omega$  can be seen as the maximal frequencies of Alfvén, gravity and  
 399 inertial waves, respectively (we return to this later).

400 For the stability analysis of system (2.23), we perform an asymptotic analysis to leading  
 401 order in  $\varepsilon$  to determine the maximal growth rates of instability (if it exists). In addition, we  
 402 integrate numerically (using the fourth-order Runge-Kutta-Gill method) system (2.23) from  
 403  $\tau = 0$  to  $\tau = 2\pi$  and we determine the eigenvalues of the solution matrix numerically (using  
 404 the double QR method).

### 405 3. Destabilised resonances of MIG waves

406 In this section, we start from the case of a vertically stratified flow with (horizontal) circular  
 407 streamlines subjected to a vertical magnetic field. In that case, there are MIG waves. We  
 408 characterise the resonant cases of these waves because some of them become destabilising  
 409 when the streamlines are elliptical ( $\varepsilon \neq 0$ ). We perform an asymptotic analysis to leading  
 410 order in  $\varepsilon$  of the Floquet system (2.23) and determine the maximal growth rate of the  
 411 destabilising resonant cases of order  $n = 2$  (called subharmonic instability). The asymptotic  
 412 analysis is performed by extending analytical techniques developed by LZ04. For the sake  
 413 of clarity, all the asymptotic calculations are reported in Appendix. Here we only state the  
 414 results.

#### 415 3.1. Dispersion relation of MIG waves

416 In this section, we establish the dispersion relation of the MIG waves propagating in a non-  
 417 diffusive unbounded fluid. The cases of inertia-gravity waves and magneto-inertia waves are  
 418 briefly addressed.

419 We denote by  $\mathbf{D}_0$  the matrix  $\mathbf{D}$  for  $E = 1$  (i.e., circular streamlines)

$$420 \quad \mathbf{D}_0 = \Omega^{-1} \begin{pmatrix} 0 & -2\Omega & i\omega_a & 0 \\ (2\Omega)^{-1}\omega_r^2 & 0 & 0 & i(\omega_a^2 + \omega_g^2)\omega_a^{-1} \\ i\omega_a & 0 & 0 & 0 \\ 0 & i\omega_a & 0 & 0 \end{pmatrix} \quad (3.1)$$

421 where

$$422 \quad \omega_r = 2\Omega \cdot (\mathbf{k}/k) = 2\Omega\mu, \quad (3.2a)$$

$$423 \quad \omega_a = \mathbf{B} \cdot \mathbf{k} = Bk_0\mu = \Omega\mathcal{B}\mu, \quad (3.2b)$$

$$424 \quad \omega_g = N|\mathbf{g} \times \mathbf{k}|/(gk) = N\sqrt{1 - \mu^2} = \Omega\mathcal{N}\sqrt{1 - \mu^2} \quad (3.2c)$$

426 are the frequencies of inertial, Alfvén and gravity waves, respectively. The eigenvalues  $\sigma_j$   
427 ( $j = 1, 2, 3, 4$ ) of the constant matrix  $\mathbf{D}_0$  take the form (Salhi *et al.* 2017),

$$428 \quad -\Omega^2 \sigma_{1,2}^2 = \omega_{1,2}^2 = \frac{1}{2} \left[ 2\omega_a^2 + \omega_r^2 + \omega_g^2 + \sqrt{(\omega_r^2 + \omega_g^2)^2 + 4\omega_r^2 \omega_a^2} \right] \quad (3.3a)$$

$$429 \quad -\Omega^2 \sigma_{3,4}^2 = \omega_{3,4}^2 = \frac{1}{2} \left[ 2\omega_a^2 + \omega_r^2 + \omega_g^2 - \sqrt{(\omega_r^2 + \omega_g^2)^2 + 4\omega_r^2 \omega_a^2} \right], \quad (3.3b)$$

431 or equivalently,

$$432 \quad \omega_1 = -\omega_2 = \frac{\Omega}{\sqrt{2}} \sqrt{(4 + 2\mathcal{B}^2 - \mathcal{N}^2) \mu^2 + \mathcal{N}^2 + \sqrt{[(4 - \mathcal{N}^2) \mu^2 + \mathcal{N}^2]^2 + 16\mathcal{B}^2 \mu^4}} \quad (3.4a)$$

$$433 \quad \omega_3 = -\omega_4 = \frac{\Omega}{\sqrt{2}} \sqrt{(4 + 2\mathcal{B}^2 - \mathcal{N}^2) \mu^2 + \mathcal{N}^2 - \sqrt{[(4 - \mathcal{N}^2) \mu^2 + \mathcal{N}^2]^2 + 16\mathcal{B}^2 \mu^4}} \quad (3.4b)$$

434 These are distinct and non-zero as long as

$$\mathcal{B} \neq 0, \quad \text{and} \quad 0 < \mu^2 < 1.$$

435 In the non-stratified case ( $\mathcal{N} = 0$ ), the frequencies  $\omega_{1,2,3,4}$  are linear with respect to the  
436 variable  $\mu$  (see equation (3.7)); in the presence of stratification, they are not. This has  
437 the consequence of making the asymptotic analysis calculations much more complex (see  
438 Appendix) than in the cases without stratification which were studied by LZ04 (the magneto-  
439 elliptical instability) and Mizerski & Bajer (2009) (the magneto-elliptical instability of  
440 rotating systems).

441 On the other hand, we note that (3.3), which can be rewritten as follows (Salhi *et al.* 2017)

$$442 \quad (\omega^2 - \omega_g^2) (\omega^2 - \omega_a^2 - \omega_g^2) - \omega_r^2 \omega^2 = 0, \quad (3.5)$$

443 represents the dispersion relation for MIG waves in a non-diffusive fluid. As it was discussed  
444 in Salhi *et al.* (2017), the dispersion relation (3.5) remains similar to that one of  $f$ -plane  
445 MHD (Schecter *et al.* 2001).

446 We can gain insight into the analysis of resonant cases of MIG waves by examining some  
447 limiting cases.

### 448 3.1.1. Inertia-gravity waves.

449 In the absence of unperturbed magnetic field ( $\mathcal{B} = 0$ , so that,  $\omega_a = 0$ ), the frequency  $\omega_{3,4}$   
450 given by (3.3) vanishes, whereas the frequency  $\omega_{1,2}$  reduces to

$$451 \quad \omega_{1,2} = \pm \sqrt{\omega_g^2 + \omega_r^2} = \Omega \sqrt{(4 - \mathcal{N}^2) \mu^2 + \mathcal{N}^2}. \quad (3.6)$$

452 In that case, there are inertia-gravity waves where the simultaneous presence of the solid-  
453 body rotation and stable vertical stratification produces higher-frequency waves because  
454  $\omega_r^2 \leq \omega_{1,2}^2$  and  $\omega_g^2 \leq \omega_{1,2}^2$ .

455 3.1.2. *Magneto-inertia waves*

456 . In the non-stratified case,  $N = 0$ , the frequency of gravity waves vanishes,  $\omega_g = 0$ . In that  
457 case, there are fast and slow magneto-inertia waves with frequency

$$458 \quad \omega_{1,2} = \pm \frac{1}{2} \left( \sqrt{\omega_r^2 + 4\omega_a^2} + \omega_r \right) = \pm \Omega \left( \sqrt{1 + \mathcal{B}^2} + 1 \right) \mu \quad (3.7a)$$

$$459 \quad \omega_{3,4} = \pm \frac{1}{2} \left( \sqrt{\omega_r^2 + 4\omega_a^2} - \omega_r \right) = \pm \Omega \left( \sqrt{1 + \mathcal{B}^2} - 1 \right) \mu, \quad (3.7b)$$

460

461 respectively. Note that, in the study by LZ04, the fast magneto-inertia waves are called  
462 “hydrodynamic modes” and the slow magneto-inertia waves are called “magnetic modes”  
463 because  $\omega_{3,4} = 0$  at vanishing unperturbed magnetic field.

464 3.2. *Resonant cases of MIG waves*

465 In this section, we establish the condition of resonances of order  $n$  between two fast or  
466 between two slow modes or between a fast mode and a slow mode.

467 The resonant cases of MIG waves are those parameter values  $(\mu, \mathcal{N}, \mathcal{B}, )$  such that

$$468 \quad \omega_i - \omega_j = n\Omega, \quad (i \neq j) \quad (3.8)$$

469 where  $n$  is an integer. For the elliptical flow, the only resonant cases that can lead to instability  
470 are those for which the integer  $n$  is even.

471 By using (3.3) we deduce that the resonance condition between two fast modes ( $\omega_1 - \omega_2 =$   
472  $n\Omega$ ) or between two slow modes ( $\omega_3 - \omega_4 = n\Omega$ ) is described by the following algebraic  
473 equation,

$$474 \quad 4\mathcal{B}^2 \left( \mathcal{B}^2 - \mathcal{N}^2 \right) \mu^4 + \left( 4\mathcal{B}^2 \mathcal{N}^2 - 2n^2 \mathcal{B}^2 - 4n^2 + n^2 \mathcal{N}^2 \right) \mu^2 + n^2 \left( \frac{n^2}{4} - \mathcal{N}^2 \right) = 0. \quad (3.9)$$

475 with  $0 < \mu^2 < 1$ . Because the replacement  $\mu \rightarrow -\mu$  and/or  $n \rightarrow -n$  in Eq. (3.9) result in the  
476 same condition, we may therefore assume without loss of generality that  $\mu > 0$  and  $n > 0$ .

477 The condition (3.9) for resonance readily extends that by Bayly (1986) for basic elliptical  
478 flow instability ( $\mathcal{B} = 0$  and  $\mathcal{N} = 0$ ). Note that  $\pi/\Omega$  is the typical time (period) for a wave  
479 packet to run the closed elliptical streamline, in the limit of vanishing, but non-zero,  $\varepsilon$ ; in the  
480 same limit, this period characterises the periodic alignment of the fluctuating vorticity with  
481 the mean (weak) strain, as  $2\pi/\omega$ . The condition can be written  $4\Omega\mu = n\Omega$  from the seminal  
482 study (Bayly 1986), that immediately yielded  $\mu = n/4 = 0.5$  (because only  $n = 2$  gives rise  
483 to  $\mu < 1$ ), giving the origin of time-dependent instability tongues at vanishing  $\varepsilon$ . Even if a  
484 single-mode analysis is apparently sufficient, as emphasised by Craik & Criminale (1986)  
485 without the need for nonlinearity (exact solution), a two-mode resonance is implied, as also  
486 suggested by the classical normal mode analysis. For both basic elliptical flow instability and  
487 precessional instability, we have to consider the modes with dispersion law  $\omega_1 = +\omega_r$  and  
488  $\omega_2 = -\omega_r$ , and the subharmonic destabilising resonance is found for  $\omega_1 - \omega_2 = 2\omega_r = \pm n\Omega$ .  
489 Accordingly, the subharmonic order is  $n = 2$  for the basic elliptical flow instability, and  
490  $n = 1$  for the precessional instability. Also in agreement with his *triad instability principle*,  
491 a detailed analysis of Waleffe (1992) shows that the elliptical instability corresponds to a  
492 forward F-interaction: the two modes with eigenfrequency  $\omega_1$  and  $\omega_2$  have opposite polarities  
493 and are coupled with the mean flow, which is associated to a zero frequency, the unstable  
494 modes are thereby two resonant inertial waves associated with the uniform background  
495 rotation.

496 In a similar manner, we determine from equation (3.3) the resonance condition between a

497 fast mode and a slow mode ( $\omega_1 - \omega_3 = n\Omega$  or  $\omega_1 - \omega_4 = n\Omega$ ),

498 
$$\left[ (4 - \mathcal{N}^2)^2 + 16\mathcal{B}^2 \right] \mu^4 - 2 \left[ 2n^2\mathcal{B}^2 + (\mathcal{N}^2 - 4)(\mathcal{N}^2 - n^2) \right] \mu^2 + (\mathcal{N}^2 - n^2)^2 = 0. \quad (3.10)$$

499 In the three following sections, we present asymptotic formulae for the maximal growth  
500 rates of the subharmonic instabilities (those corresponding to the destabilising resonances of  
501 order  $n = 2$ ). The asymptotic formulae are yielded by the asymptotic analysis at leading  
502 order in  $\varepsilon$  of the Floquet system (2.23). Obviously, the instabilities related to higher-  
503 order resonances ( $n = 4, 6, 8, \dots$ ) are excluded by the procedure leading to the asymptotic  
504 formulae. These instabilities (if they exist) can be captured by the numerical computations  
505 (see section 4).

### 506 3.3. Destabilising resonance between two fast modes

507 As shown by LZ04, the universal elliptic instability, which results from the resonances (of  
508 order  $n = 2$ ) between two fast modes, persists in the presence of magnetic fields of arbitrary  
509 strength, although the growth rate decreases somewhat (LZ04). As a counterpart, in the  
510 presence of vertical (stable) stratification, it is completely suppressed when  $\mathcal{N}$  reaches 1  
511 (Miyazaki & Fukumoto 1992). In this section, we investigate the effects of the axial (stable)  
512 stratification and magnetic field when there are simultaneously present on this instability  
513 (referred to as IF instability).

514 A detailed analysis of the algebraic equation (3.9), knowing that  $0 \leq \mu^2 \leq 1$ ,  $0 \leq \mathcal{B} < +\infty$   
515 and  $0 \leq \mathcal{N} < +\infty$ , indicates that the resonant case of order  $n = 2$  between two fast modes  
516 ( $\omega_1 - \omega_2 = 2\Omega$ ) exists for

517 
$$(\mathcal{B}, \mathcal{N}) \in ([0, +\infty[ \times [0, 1]) \cup \mathcal{D}_f \quad (3.11)$$

518 which corresponds to the domains I, II and VI of the plane  $(\mathcal{B}, \mathcal{N})$  shown by figure 2. Here,  
519 the domain  $\mathcal{D}_f$  is defined as follows:

520 
$$\forall (\mathcal{B}, \mathcal{N}) \in \mathcal{D}_f \Leftrightarrow \text{for given } \mathcal{N} \in ]2, +\infty[ \implies 1 < f(\mathcal{N}) \leq \mathcal{B} < \sqrt{3}, \quad (3.12)$$

521 where  $f : ]2, +\infty[ \rightarrow ]1, \sqrt{3}[$  is a continuous decreasing function with reciprocal function  
522  $f^{-1} : ]1, \sqrt{3}[ \rightarrow ]2, +\infty[$ ,

523 
$$\forall \mathcal{N} \in ]2, +\infty[, f(\mathcal{N}) = \frac{1}{\mathcal{N}^2} \sqrt{\mathcal{N}^4 + 4\mathcal{N}^2 - 8 + 4\sqrt{(\mathcal{N}^2 - 1)(\mathcal{N}^4 - 4)}} \xrightarrow{\mathcal{N} \rightarrow +\infty} 1, \quad (3.13a)$$

524 
$$\forall \mathcal{B} \in ]1, \sqrt{3}[, f^{-1}(\mathcal{B}) = \frac{2}{(\mathcal{B}^2 - 1)} \sqrt{1 + \mathcal{B}^2 + \mathcal{B}\sqrt{4 - (\mathcal{B}^2 - 1)^2}} \xrightarrow{\mathcal{B} \rightarrow 1^+} +\infty. \quad (3.13b)$$

526 For  $(\mathcal{B}, \mathcal{N})$  belonging to the domain given by (3.11), the resonances (of order  $n = 2$ ) between  
527 two fast modes occur when

528 
$$\mu^2 = \frac{1 - \mathcal{N}^2}{4 - \mathcal{N}^2} \quad \text{if } \mathcal{B} = 0, \quad (3.14a)$$

529 
$$\mu^2 = \frac{\mathcal{B}^2 - 1}{\mathcal{B}^4 - \mathcal{B}^2 - 4} \quad \text{if } \mathcal{B} = \mathcal{N}, \quad (3.14b)$$

530 
$$\mu^2 = \frac{(1 + \mathcal{B}^2)(1 - \mathcal{N}^2) + \mathcal{B}^2 + 3 - \sqrt{\Delta}}{2\mathcal{B}^2(\mathcal{B}^2 - \mathcal{N}^2)} \quad \text{if } \mathcal{B} \neq \mathcal{N}, \quad (3.14c)$$

532 where

533 
$$\Delta(\mathcal{B}, \mathcal{N}) = \left( \mathcal{N}^2 (\mathcal{B}^2 - 1) - 4 \right)^2 + 16 (\mathcal{B}^2 - \mathcal{N}^2). \quad (3.15)$$

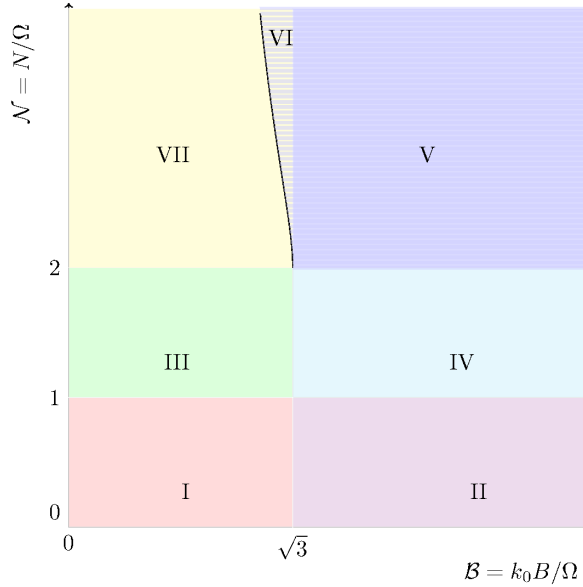


Figure 2

Domains of the  $(\mathcal{B}, \mathcal{N})$  plane for which the magneto-gravity-elliptic instability operates. The subharmonic instability resulting from a resonance (of order  $n = 2$ ) between two fast modes (referred to as IF instability) exists for  $(\mathcal{B}, \mathcal{N})$  belonging to domains I, II and VI. The subharmonic instability resulting from a resonance between two slow modes (referred to as IS instability) exists for  $(\mathcal{B}, \mathcal{N})$  belonging to domains II, IV, V and VI. The subharmonic instability resulting from a resonance between a fast mode and a slow mode (referred to as IM instability) exists for  $(\mathcal{B}, \mathcal{N})$  belonging to domains I, II, III and IV. For  $(\mathcal{B}, \mathcal{N})$  belonging to domain VII, there is no subharmonic instability, whereas instabilities related to higher order resonances ( $n = 4, 6, 8, \dots$ ) can exist.

Domain I:  $(\mathcal{B}, \mathcal{N}) \in [0, \sqrt{3}] \times [0, 1]$ ; domain II:  $(\mathcal{B}, \mathcal{N}) \in [\sqrt{3}, +\infty[ \times [0, 1]$ ; domain III:  $(\mathcal{B}, \mathcal{N}) \in [0, \sqrt{3}] \times [1, 2]$ ; domain IV:  $(\mathcal{B}, \mathcal{N}) \in [\sqrt{3}, +\infty[ \times [1, 2]$ ; domain V:  $(\mathcal{B}, \mathcal{N}) \in [\sqrt{3}, +\infty[ \times [2, +\infty[$ ; domain VI:  $(\mathcal{B}, \mathcal{N}) \in \mathcal{D}_f$  where  $\mathcal{D}_f$  is defined by equation (3.12); domain VII:  $(\mathcal{B}, \mathcal{N}) \in [0, \sqrt{3}] \times [2, +\infty[ \setminus \mathcal{D}_f$ .

534 It immediately follows that

$$535 \quad \lim_{0 \leq \mathcal{N} \leq 1, \mathcal{B} \rightarrow +\infty} \mathcal{B}^2 \mu^2 = 1 - \mathcal{N}^2, \quad \lim_{1 < \mathcal{B} < \sqrt{3}, \mathcal{N} \rightarrow +\infty} \mathcal{B}^2 \mu^2 = 1. \quad (3.16)$$

536 In the non-stratified magnetised case ( $\mathcal{N} = 0$ ), the parameter  $\mu = [1 + \sqrt{1 + \mathcal{B}^2}]^{-1}$  changes  
 537 from 0.5 (so that,  $\theta = (\mathbf{k}, \mathbf{W}) = \cos^{-1}(\mu) = \pi/3$ ) at  $\mathcal{B} = 0$  to zero (so that,  $\theta = \pi/2$ ) as  
 538  $\mathcal{B} \rightarrow +\infty$  (see also LZ04). Recall that  $\mathbf{k}$  denotes the wave vector and  $\mathbf{W} = \nabla \times \mathbf{U}$  denotes  
 539 the basic vorticity vector. In the non-magnetised stratified case ( $\mathcal{B} = 0$ ), the parameter  
 540  $\mu = \sqrt{(1 - \mathcal{N}^2)/(4 - \mathcal{N}^2)}$  changes from  $\mu = 0.5$  at  $\mathcal{N} = 0$  to  $\mu = 0$  at  $\mathcal{N} = 1$ . For  $(\mathcal{B}, \mathcal{N}) \in$   
 541  $[0, +\infty[ \times [0, 1]$  and when  $\mathcal{B}$  is fixed, the parameter  $\mu$  changes from  $\mu = [1 + \sqrt{1 + \mathcal{B}^2}]^{-1}$  at  
 542  $\mathcal{N} = 0$  to  $\mu = 0$  at  $\mathcal{N} = 1$ . For  $(\mathcal{B}, \mathcal{N}) \in \mathcal{D}_f$  and when  $\mathcal{B}$  is fixed, the parameter  $\mu$  increases  
 543 from  $\mu(\mathcal{B}, f(\mathcal{B}))$  at  $\mathcal{N} = f(\mathcal{B})$  to  $\mu = 1$  as  $\mathcal{N} \rightarrow +\infty$ . As an illustration, figure 3 shows the  
 544 variation of  $\mu$  versus  $\mathcal{N}$  for three values of  $\mathcal{B} = \sqrt{3}, 1.632, 1.532$ .

545 According to our asymptotic analysis at leading order in  $\varepsilon$  (see Appendix), the maximal  
 546 growth rate of the subharmonic instability (if it exists) resulting from the resonance between



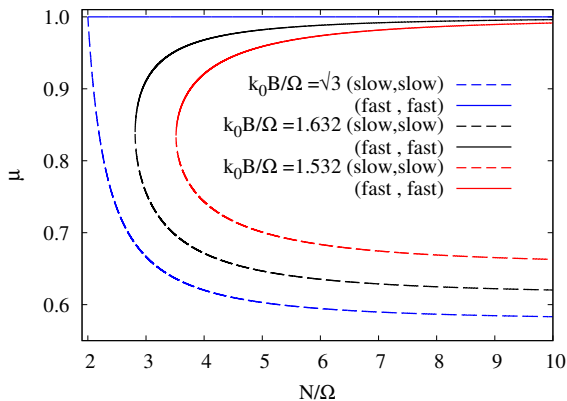


Figure 3

Resonant cases of order  $n = 2$  in the case where  $(\mathcal{B}, \mathcal{N}) \in \mathcal{D}_f$  (see equation (3.12)). Variation of  $\mu = \cos(\theta) = k_3/k_0$  versus  $\mathcal{N} = N/\Omega$  for  $\mathcal{B} = k_0B/\Omega = \sqrt{3}, 1.632$  and  $\mathcal{B} = 1.532$ . Solid lines represent the resonances between two fast modes (fast, fast) and dotted lines represent the resonances between two slow modes (slow, slow).

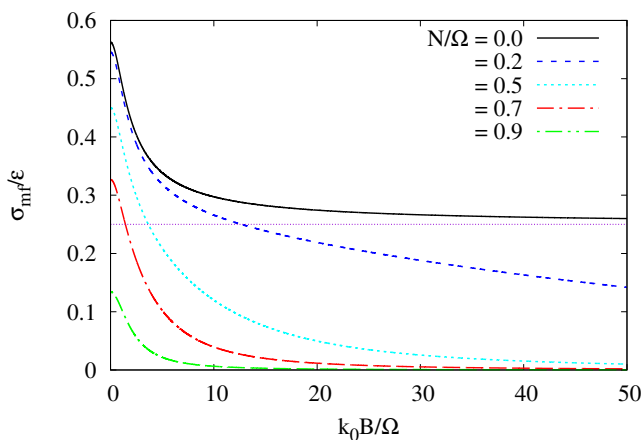


Figure 4

Maximal growth rate of the destabilising resonances of order  $n = 2$  between two fast modes (see equation (3.17)). The figure shows  $\sigma_{mf}/\varepsilon$  versus  $\mathcal{B} = k_0B/\Omega$  for  $\mathcal{N} = N/\Omega = 0., 0.2, 0.5, 0.7$  and  $\mathcal{N} = 0.9$ .

547 two fast modes is of the form

$$548 \quad \frac{\sigma_{mf}}{\varepsilon} = \frac{(3 - \mathcal{B}^2\mu^2)(1 + \mathcal{B}^2\mu^2)}{8} \frac{[(\mathcal{N}^2 - \mathcal{B}^2 + 2)\mu^2 + (1 - \mathcal{N}^2)]}{[(\mathcal{N}^2 - 2\mathcal{B}^2 - 4)\mu^2 + (2 - \mathcal{N}^2)]} \quad (3.17)$$

549 in which  $\mu^2$  is given by equation (3.14).

550 Some results reported in previous studies (Waleffe (1990); Kerswell (2002) and LZ04)

551 can be recovered from equation (3.17) by using (3.14)

$$552 \quad \frac{\sigma_{mf}}{\varepsilon} = \frac{9}{16} \quad \text{for } \mathcal{N} = 0, \mathcal{B} = 0, \quad (3.18a)$$

$$553 \quad \frac{\sigma_{mf}}{\varepsilon} = \frac{9(1 - \mathcal{N}^2)}{4(4 - \mathcal{N}^2)} \quad \text{for } 0 \leq \mathcal{N} \leq 1, \mathcal{B} = 0, \quad (3.18b)$$

$$554 \quad \frac{\sigma_{mf}}{\varepsilon} = \frac{1}{4} \left( 1 + \frac{1}{\sqrt{\mathcal{B}^2 + 1} + 1} \right)^2 \quad \text{for } \mathcal{N} = 0, 0 \leq \mathcal{B} < +\infty. \quad (3.18c)$$

556 Equation (3.18b) indicates that the maximal growth rate is zero at  $\mathcal{N} = 1$ . Therefore in the  
557 non-magnetised stratified case ( $\mathcal{B} = 0$ ), the subharmonic instability is completely suppressed  
558 by stratification when  $\mathcal{N}$  reaches 1 (Miyazaki & Fukumoto 1992; Kerswell 2002). For the  
559 non-stratified magnetised case ( $\mathcal{N} = 0$ ), equation (3.18c) indicates that  $\sigma_{mf}/\varepsilon$  decreases as  
560  $\mathcal{B}$  increases so as (see also LZ04)

$$561 \quad \lim_{\mathcal{N}=0, \mathcal{B} \rightarrow +\infty} \frac{\sigma_{mf}}{\varepsilon} = \frac{1}{4}. \quad (3.19)$$

562 However, in the stratified magnetised case, the analysis of equation (3.17) is more subtle as  
563 shown in the following.

564 For  $(\mathcal{B}, \mathcal{N}) \in ]0, +\infty[ \times ]0, 1]$  and when  $\mathcal{N}$  is fixed,  $\sigma_{mf}/\varepsilon$  also decreases from  $\sigma_{mf}/\varepsilon =$   
565  $[9(1 - \mathcal{N}^2)]/[4(4 - \mathcal{N}^2)]$  at  $\mathcal{B} = 0$  to zero (and not to 1/4) as  $\mathcal{B} \rightarrow +\infty$ . Indeed, from  
566 equation (3.17), one easily deduces that

$$567 \quad \lim_{0 < \mathcal{N} \leq 1, \mathcal{B} \rightarrow +\infty} \frac{\sigma_{mf}}{\varepsilon} = 0, \quad (3.20)$$

568 because  $\lim_{\mathcal{B} \rightarrow +\infty} \mathcal{B}^2 \mu^2 = 1 - \mathcal{N}^2$ , as indicated previously. Therefore, the  $\mathcal{N} \rightarrow 0$  limit is,  
569 in fact, singular (discontinuous). As an illustration, figure 4 shows  $\sigma_{mf}/\varepsilon$  versus  $\mathcal{B}$  for five  
570 values of  $\mathcal{N} = 0.0, 0.2, 0.5, 0.7, 0.9$ . At  $\mathcal{N} = 1$ , one has  $\sigma_{mf} = 0$  independently of  $\mathcal{B}$ .

571 For  $(\mathcal{B}, \mathcal{N}) \in \mathcal{D}_f$  and for fixed  $\mathcal{N}$ , the maximal growth rate  $\sigma_{mf}$  increases from 0 at  
572  $\mathcal{B} = \sqrt{3}$  to  $\sigma_{mf}(f(\mathcal{N}), \mathcal{N})$  at  $\mathcal{B} = f(\mathcal{N})$  with

$$573 \quad \lim_{\mathcal{N} \rightarrow +\infty} \frac{\sigma_{fm}(f(\mathcal{N}), \mathcal{N})}{\varepsilon} = \frac{1}{2}. \quad (3.21)$$

This is illustrated by figure 5 which displays the variation of  $\sigma_{mf}/\varepsilon$  versus  $\mathcal{B}$  ( $1 < \mathcal{B} < \sqrt{3}$ )  
for  $\mathcal{N} = 10$  and  $\mathcal{N} = 50$ . Therefore, this subharmonic instability, which occurs when

$$2\Omega < N < +\infty \quad \text{and} \quad \Omega < k_0 B = \Omega f(\mathcal{N}) < \sqrt{3} \Omega,$$

574 is the results of the simultaneous presence of axial (stable) stratification and magnetic field.  
575 On the other hand, the above analysis clearly shows that, for  $(\mathcal{B}, \mathcal{N}) \in [0, +\infty[ \times ]0, 1]$ ,  
576 the IF instability is completely suppressed by the stratification when  $\mathcal{N}$  reaches 1. When  
577  $0 < \mathcal{N} < 1$ , stratification acts to render the IF instability less efficient especially for large  $\mathcal{B}$   
578 because its maximal growth approaches zero as  $\mathcal{B} \rightarrow +\infty$  (see equation (3.20)).

#### 579 3.4. Destabilising resonances between two slow modes

580 As shown by LZ04, in the presence only of the magnetic field, there exist other subharmonic  
581 instabilities, which are due to the presence of the magnetic field, in addition to the universal  
582 elliptical instability. One of them is the subharmonic instability resulting from the resonances  
583 (of order  $n = 2$ ) between two slow modes (referred to as IS instability). In this section, we  
584 study the effects of the vertical (stable) stratification on the IS instability.

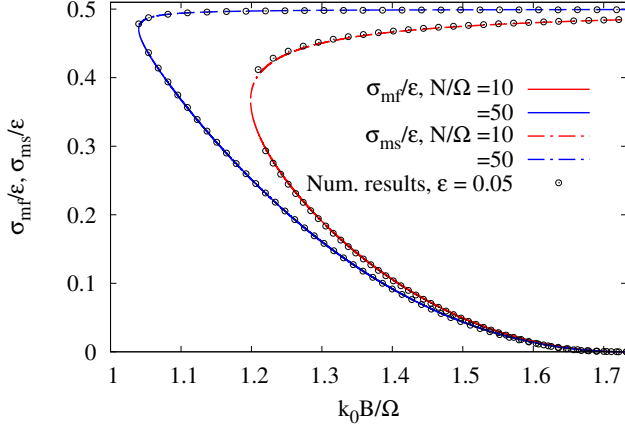


Figure 5

Maximal growth rates of subharmonic instabilities resulting from the resonances between two fast modes ( $\sigma_{mf}$ ) or between two slow modes ( $\sigma_{ms}$ ) in the case where  $(\mathcal{B}, \mathcal{N}) \in \mathcal{D}_f$  (see equation (3.12)). The figure shows the variation of  $\sigma_{mf}/\epsilon$  and  $\sigma_{ms}/\epsilon$  versus  $\mathcal{B} = k_0 B/\Omega$  for  $\mathcal{N} = \mathcal{N}/\Omega = 10$  and  $\mathcal{N} = 50$ . Numerical results (see section 4) for  $\epsilon = 0.05$  are represented by symbols.

585 From the resonant condition described by relation (3.9), we deduce that the resonant cases  
586 of order  $n = 2$  between two slow modes, so that  $\omega_3 - \omega_4 = 2\Omega$ , exist for

$$587 \quad (\mathcal{B}, \mathcal{N}) \in \left( [\sqrt{3}, +\infty[ \times [0, +\infty[ \right) \cup \mathcal{D}_f \quad (3.22)$$

588 This corresponds to the domains II, IV, V and VI shown in figure 2.

589 For  $(\mathcal{B}, \mathcal{N})$  belonging to these domains, the resonant cases of order  $n = 2$  between two  
590 slow modes occur at the following points of the  $\mu$  axis

$$591 \quad \mu^2 = \frac{\mathcal{B}^2 - 1}{\mathcal{B}^4 - \mathcal{B}^2 - 4} \quad \text{if } \mathcal{B} = \mathcal{N}, \quad (3.23a)$$

$$592 \quad \mu^2 = \frac{(1 + \mathcal{B}^2)(1 - \mathcal{N}^2) + \mathcal{B}^2 + 3 + \sqrt{\Delta}}{2\mathcal{B}^2(\mathcal{B}^2 - \mathcal{N}^2)} \quad \text{if } \mathcal{B} \neq \mathcal{N} \quad (3.23b)$$

594 It immediately follows that

$$595 \quad \lim_{\mathcal{N} \geq 0, \mathcal{B} \rightarrow +\infty} \mu^2 \mathcal{B}^2 = 1, \quad \lim_{\mathcal{B} > 1, \mathcal{N} \rightarrow +\infty} \mu^2 \mathcal{B}^2 = 1. \quad (3.24)$$

596 In the non-stratified magnetised case, equation (3.23) reduces to  $\mu = [\sqrt{\mathcal{B}^2 + 1} - 1]^{-1}$ , or  
597 equivalently,  $\mu^2 \mathcal{B}^2 = 1 + 2\mu$ . Thus, the parameter  $\mu$  changes from 1 at  $\mathcal{B} = \sqrt{3}$  to 0 as  $\mathcal{B} \rightarrow +\infty$   
598 (see also LZ04). In the stratified magnetised case, equation (3.23) indicates that, at fixed  $\mathcal{B}$   
599 such that  $(\mathcal{B}, \mathcal{N}) \in [\sqrt{3}, +\infty[ \times [0, +\infty[$ , the parameter  $\mu$  changes from  $\mu = [\sqrt{\mathcal{B}^2 + 1} - 1]^{-1}$   
600 at  $\mathcal{N} = 0$  to  $\mu = 1/\mathcal{B}$  as  $\mathcal{N} \rightarrow +\infty$ . For fixed  $\mathcal{B}$  such that  $(\mathcal{B}, \mathcal{N}) \in \mathcal{D}_f$ , the parameter  $\mu$   
601 decreases from  $\mu(\mathcal{B}, f(\mathcal{B}))$  at  $\mathcal{N} = f(\mathcal{B})$  to  $\mu = 1/\mathcal{B}$  as  $\mathcal{N} \rightarrow +\infty$  (see figure 3).

602 As shown in Appendix, the maximal growth rate, denoted by  $\sigma_{ms}$ , of the IS instability is  
603 also described by equation (3.17) (repeated here for the sake of clarity)

$$604 \quad \frac{\sigma_{ms}}{\epsilon} = \frac{(3 - \mathcal{B}^2 \mu^2)(1 + \mathcal{B}^2 \mu^2)}{8} \frac{[(\mathcal{N}^2 - \mathcal{B}^2 + 2)\mu^2 + (1 - \mathcal{N}^2)]}{[(\mathcal{N}^2 - 2\mathcal{B}^2 - 4)\mu^2 + (2 - \mathcal{N}^2)]} \quad (3.25)$$

605 in which  $\mu$  is now given by equation (3.23) and not by (3.14).

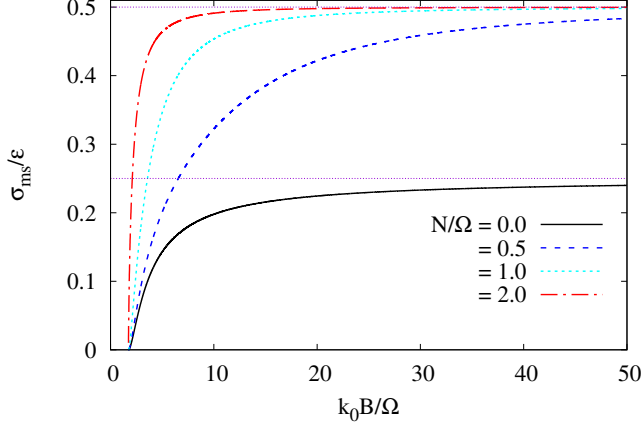


Figure 6

Maximal growth rate of the destabilising resonances of order  $n = 2$  between two slow modes (see equation (3.25)). The figure shows  $\sigma_{ms}/\varepsilon$  versus  $\mathcal{B}$  for  $N = 0., 0.5, 1., 2$  and  $N = 3$ .

606 In the non-stratified magnetised case ( $N = 0$ ), equation (3.25) reduces to

$$607 \quad \frac{\sigma_{ms}}{\varepsilon} = \frac{1}{4} \left( 1 - \frac{1}{\sqrt{\mathcal{B}^2 + 1} - 1} \right)^2 \xrightarrow{N=0, \mathcal{B} \rightarrow +\infty} \frac{1}{4}, \quad (3.26)$$

608 where  $\sqrt{3} < \mathcal{B} < +\infty$ , in agreement with the previous results by LZ04. In that case,  $\sigma_{ms}/\varepsilon$   
609 increases from 0 at  $\mathcal{B} = \sqrt{3}$  to  $1/4$  as  $\mathcal{B} \rightarrow +\infty$ .

610 For  $(\mathcal{B}, N) \in ([\sqrt{3}, +\infty[ \times [0, +\infty[) \cup \mathcal{D}_f$ , we use the equation (3.24) to deduce from  
611 equation (3.25) the following limits

$$612 \quad \lim_{N>0, \mathcal{B} \rightarrow +\infty} \frac{\sigma_{ms}}{\varepsilon} = \frac{1}{2}, \quad \lim_{\mathcal{B}>1, N \rightarrow +\infty} \frac{\sigma_{ms}}{\varepsilon} = \frac{1}{2}. \quad (3.27)$$

613 Indeed, when  $\mathcal{B} \gg 1$  and  $\mathcal{B} \gg N > 0$ , an equivalent form for  $\sigma_{ms}/\varepsilon$  can be written as

$$614 \quad \frac{\sigma_{ms}}{\varepsilon} \underset{\mathcal{B} \rightarrow +\infty}{\sim} \frac{(3 - \mathcal{B}^2 \mu^2)(1 + \mathcal{B}^2 \mu^2)}{8} \frac{(1 - N^2 - \mathcal{B}^2 \mu^2)}{(2 - N^2 - 2\mathcal{B}^2 \mu^2)} \xrightarrow{\mathcal{B} \rightarrow +\infty} \frac{1}{2} \quad (3.28)$$

615 because  $\lim_{\mathcal{B} \rightarrow +\infty} \mu^2 \mathcal{B}^2 = 1$ . When  $N \gg \mathcal{B} > 1$ , an equivalent form for  $\sigma_{ms}/\varepsilon$  can be  
616 written as

$$617 \quad \frac{\sigma_{ms}}{\varepsilon} \underset{N \rightarrow +\infty}{\sim} \frac{(3 - \mathcal{B}^2 \mu^2)(1 + \mathcal{B}^2 \mu^2)}{8} \xrightarrow{N \rightarrow +\infty} \frac{1}{2} \quad (3.29)$$

618 because  $\lim_{N \rightarrow +\infty} \mu^2 \mathcal{B}^2 = 1$ .

619 It follows that, for  $(\mathcal{B}, N) \in [\sqrt{3}, +\infty[ \times [0, +2]$  and when  $N$  is fixed,  $\sigma_{ms}/\varepsilon$  increases  
620 from 0 at  $\mathcal{B} = \sqrt{3}$  to 0.5 as  $\mathcal{B} \rightarrow +\infty$ . This is illustrated by figure 6 which shows  $\sigma_{ms}/\varepsilon$   
621 versus  $\mathcal{B}$  for  $N = 0, 0.5, 1$  and  $N = 2$ . By comparing (3.26) and (3.29), we can remark that,  
622 in this case, the  $N \rightarrow 0$  limit is, in fact, singular (discontinuous). Consequently, we can  
623 conclude that in the presence of the stratification with  $N \leq 2$  the IS instability is reinforced  
624 since  $\sigma_{ms}/\varepsilon$  tends towards  $1/2$  like  $\mathcal{B} \rightarrow +\infty$ , whereas without stratification ( $N = 0$ ),  $\sigma_{ms}/\varepsilon$   
625 approaches  $1/4$ .

626 On the other hand, for  $(\mathcal{B}, N) \in \mathcal{D}_f \cup ([\sqrt{3}, +\infty[ \times [2, +\infty[)$  (this corresponds to the

627 domains V and VI shown in figure 2) and when  $\mathcal{N}$  is fixed,  $\sigma_{ms}/\varepsilon$  also increases from  
 628  $\sigma_{mf}(f(\mathcal{N}), \mathcal{N})/\varepsilon$  at  $\mathcal{B} = f(\mathcal{N})$  to 0.5 as  $\mathcal{B} \rightarrow +\infty$ . Indeed, for  $(\mathcal{B}_1, \mathcal{N}) \in \mathcal{D}_f$  and  
 629  $(\mathcal{B}_2, \mathcal{N}) \in [\sqrt{3}, +\infty[ \times ]2, +\infty[$ , we have (see figure 5),

$$630 \quad 0 \leq \sigma_{mf}(\mathcal{B}_1, \mathcal{N}) \leq \sigma_{ms}(\mathcal{B}_1, \mathcal{N}) \leq \sigma_{ms}(\mathcal{B}_2, \mathcal{N}) < \frac{\varepsilon}{2}. \quad (3.30)$$

631 It clearly appears that in the simultaneous presence of the axial magnetic field and strati-  
 632 fication with  $\mathcal{N} > 2$ , the subharmonic instability resulting from the resonances (of order  
 633  $n = 2$ ) between two slow modes, which emerges beyond the threshold  $\mathcal{B}_c = f(\mathcal{N}) < \sqrt{3}$ , is  
 634 dominant with a maximal growth rate approaching  $\varepsilon/2$  for large  $\mathcal{B}$ .

### 635 3.5. Destabilising resonances between a fast mode and a slow mode

636 In this section, we study the effects of the vertical (stable) stratification on the subharmonic  
 637 instability resulting from the resonances (of order  $n = 2$ ) between a fast mode and a slow  
 638 mode (hereinafter, referred to as IM instability). Without stratification, the IM instability  
 639 occurs for all magnetic field strengths where its maximal growth rate approaches  $\varepsilon/4$  as  
 640  $\mathcal{B} \rightarrow +\infty$  (see LZ04).

The resonance of order  $n = 2$  between a fast mode and a slow mode, i.e.  $\omega_1 - \omega_3 = 2\Omega$  or  
 $\omega_1 - \omega_4 = 2\Omega$ , exists for

$$(\mathcal{B}, \mathcal{N}) \in ]0, +\infty[ \times ]0, +\infty[.$$

641 In the case where  $\omega_1 - \omega_4 = 2\Omega$ , one has  $\mu = 1$ , but this resonant case does not induce any  
 642 instability because the Floquet system (2.23) is stable at  $\mu = 1$ , as already indicated.

643 In the case where  $\omega_1 - \omega_3 = 2\Omega$ , we deduce from the algebraic equation (3.10) that the  
 644 points of the  $\mu$ -axis characterising the resonances between a fast mode and a slow mode are  
 645 given by

$$646 \quad \mu^2 = \frac{(4 - \mathcal{N}^2)^2}{(4 - \mathcal{N}^2)^2 + 16\mathcal{B}^2} \quad (3.31)$$

647 The latter expression implies that, for fixed  $\mathcal{N} \geq 0$ , the parameter  $\mu$  decreases from 1 at  
 648  $\mathcal{B} = 0$  to zero as  $\mathcal{B} \rightarrow +\infty$ . Inversely, for fixed  $\mathcal{B} > 0$ , the parameter  $\mu$  increases from  
 649  $\mu = 1/\sqrt{1 + \mathcal{B}^2}$  at  $\mathcal{N} = 0$  to 1 as  $\mathcal{N} \rightarrow +\infty$ .

650 However, according to our asymptotic analysis (see Appendix), only the resonant cases  
 651 for which the couple  $(\mathcal{B}, \mathcal{N})$  belongs to the domain  $]0, +\infty[ \times ]0, 2[$  (this corresponds to the  
 652 domains I-IV shown in figure 2), are destabilising. In that case, the maximal growth rate of  
 653 the IM instability, denoted by  $\sigma_{mm}$ , is found as (see Appendix A.3.3.)

$$654 \quad \frac{\sigma_{mm}}{\varepsilon} = \frac{(1 - \mu^2) [(1 - \mu^2)(4 - \mathcal{N}^2) + 4\mathcal{N}^2]}{16 \sqrt{4 + \mathcal{N}^2}} \sqrt{\frac{(4 - \mathcal{N}^2)^3}{(4 - \mathcal{N}^2)^2 + \mathcal{B}^2 \mathcal{N}^4}} \quad (3.32)$$

655 It immediately follows that  $\sigma_{mm} = 0$  for  $\mathcal{N} = 2$ , independently of the magnetic field strength.

656 In the non-stratified case ( $\mathcal{N} = 0$ ), Equation (3.32) reduces to

$$657 \quad \frac{\sigma_{mm}}{\varepsilon} = \frac{1}{4} \left(1 - \mu^2\right)^2 = \frac{\mathcal{B}^4}{4(1 + \mathcal{B}^2)^2} \xrightarrow{\mathcal{B} \rightarrow +\infty} \frac{1}{4}, \quad (3.33)$$

658 in agreement with the study by LZ04. Therefore,  $\sigma_{mm}/\varepsilon$  increases from 0 at  $\mathcal{B} = 0$  to  
 659 approach  $1/4$  as  $\mathcal{B} \rightarrow +\infty$ .

660 However, in the simultaneous presence of the vertical (stable) stratification and the  
 661 magnetic field and for fixed  $\mathcal{N} \leq 2$ ,  $\sigma_{mm}/\varepsilon$  increases from 0 to reach its maximum value  
 662 (which is less than  $1/4$ ), then it decreases tending towards zero when  $\mathcal{B} \rightarrow +\infty$ . Also in this

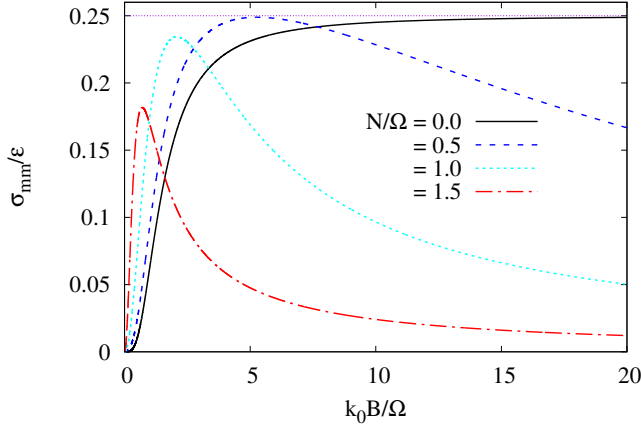


Figure 7

Maximal growth rate of the destabilising resonances of order  $n = 2$  between a fast and a slow mode (see equation (3.32)). The figure shows  $\sigma_{mm}/\varepsilon$  versus  $\mathcal{B}$  for  $\mathcal{N} = 0., 0.5, 1$  and  $\mathcal{N} = 1.5$

663 case, the  $\mathcal{N} \rightarrow 0$  limit is, in fact, singular (discontinuous). As an illustration, figure 7 shows  
 664  $\sigma_{mm}/\varepsilon$  versus  $\mathcal{B}$  for  $\mathcal{N} = 0, 0.5, 1, 1.5$  and  $\mathcal{N} = 2$ .

665 We can therefore conclude that the effect of (stable) stratification on the IM instability is  
 666 to suppress it if  $\mathcal{N}$  exceeds 2, or to make it less efficient otherwise ( $0 < \mathcal{N} < 2$ ) because  
 667  $\sigma_{mm}$  approaches zero for large  $\mathcal{B}$ .

#### 668 4. Numerical results

669 In this section, we numerically determine the maximal growth rate of the dominant instability  
 670 for a given value of the triplet  $(\mathcal{B}, \mathcal{N}, \varepsilon)$  such that  $0 \leq \mathcal{B} = B/\Omega \leq 4$  and  $0 \leq \mathcal{N} = N/\Omega \leq 4$   
 671 and  $0 \leq \varepsilon \leq 1$  (or, equivalently,  $1 \leq E = \varepsilon + \sqrt{1 + \varepsilon^2} = 1 + \sqrt{2}$ ). We use the resonance  
 672 conditions (3.9) and (3.10) for the identification of the instability (if it exists) and we compare  
 673 the asymptotic formulae with the numerical results. At the end of this section, we briefly  
 674 examine the effect of fluid diffusivity in a special case where the diffusion coefficients are  
 675 equal ( $\nu = \kappa = \eta$ ).

##### 676 4.1. Identification of instabilities

677 For the identification of the instabilities picked up by the numerical procedure we use the  
 678 resonance conditions described by equation (3.9) and (3.10) as explained as follows.

679 On the one hand, for a given value of the couple  $(\mathcal{B}, \mathcal{N})$ , we use (3.14), (3.23) and (3.31)  
 680 and determine the values of  $\mu$ , say  $\mu_0$ , characterising the resonant cases of order  $n = 2$ . On  
 681 the other hand, for the same value of the couple  $(\mathcal{B}, \mathcal{N})$ , we consider several values of  $\varepsilon$   
 682 uniformly distributed in the interval  $[0, 1]$  and, for each of these values of  $\varepsilon$ , we integrate  
 683 numerically the Floquet system (2.23) and determine the growth rate  $\sigma$  for 2000 values  
 684 of  $\mu$  (evenly distributed) in  $]0, 1[$ . Obviously,  $\sigma(\mu) = 0$  if there is no instability. Thus, in  
 685 the plane  $(\mu, \sigma + \varepsilon)$ , the region of instability that emanates from the point of abscissa  $\mu_0$   
 686 characterises a subharmonic instability. As an illustration, figure 8 shows  $\sigma + \varepsilon$  versus  $\mu$   
 687 for  $\mathcal{B} = 4$  and  $\mathcal{N} = 0.5$  and 100 values of  $\varepsilon$  evenly distributed in the interval  $[0, 0.8]$ .  
 688 In that case, there are three subharmonic instabilities IF, IM and IS which correspond to  
 689 the regions of instability emanating from the points  $(\mu_0 = 0.1755, 0)$ ,  $(\mu_0 = 0.2282, 0)$

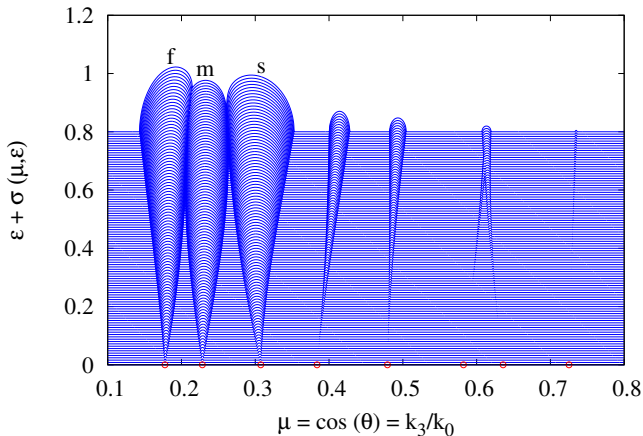


Figure 8

Magneto-gravity elliptic instabilities. The figure shows  $\sigma + \varepsilon$  versus  $\mu$  for  $\mathcal{B} = 4$  and  $\mathcal{N} = 0.5$  and 100 values of  $\varepsilon$  evenly distributed in the interval  $[0, 0.8]$ . The regions of instability labelled by f, m and s denote the IF, IM and IS instabilities that emanate from the points of the  $\mu$ -axis of abscissa 0.1775, 0.2282 and 0.3074, respectively. The other instabilities picked up by the numerical procedure are related to higher-order resonances ( $n = 4, 6, 8, \dots$ ): for  $n = 4$ ,  $\mu = 0.3836$  (fast, fast),  $\mu = 0.4792$  (fast, slow),  $\mu = 0.6359$  (slow, slow); for  $n = 6$ ,  $\mu = 0.5821$  (fast, fast),  $\mu = 0.7252$  (fast, slow).

690 and  $(\mu_0 = 3074, 0)$ , respectively. The other instabilities appearing in figure 6 are related to  
 691 higher-order resonances ( $n = 4, 6, 8, \dots$ ), but as they are dominated by the subharmonic  
 692 instabilities, we do not seek to identify them one by one.

#### 693 4.2. Comparison between the asymptotic formulae and the numerical results

We recall that the present asymptotic results (at leading order in  $\varepsilon$ ) clearly shows that subharmonic instability exists when

$$(\mathcal{B}, \mathcal{N}) \in ([0, +\infty[ \times [0, 2]) \cup \left( [\sqrt{3} + \infty[ \times [2, +\infty[ \right) \cup \mathcal{D}_f.$$

694 Obviously, the procedure leading to the asymptotic formulae excludes the instabilities related to  
 695 higher-order resonances ( $n = 4, 6, 8, \dots$ ). Numerical calculations indicate that, when  
 696  $(\mathcal{B}, \mathcal{N})$  belongs to domains I-VI (see figure 2) deprived of a very narrow band which are  
 697 specified below, one of the subharmonic instabilities listed in section 3 is dominant.

In figure 9, we show the continuous variation of the maximal growth rate  $\sigma_m$  (maximum  $\sigma$  over  $0 \leq \mu \leq 1$ ) of the dominant instability normalised by  $\sigma_0 = 9/16$  plotted as a function of  $0 \leq \mathcal{B} \leq 4$  and  $0 \leq \mathcal{N} \leq 4$ . Figure 9(a) displays the numerical results for  $\varepsilon = 0.1$ , where the grid consists of 201 points evenly distributed in each one of the ranges  $0 \leq \mathcal{B} \leq 4$  and  $0 \leq \mathcal{N} \leq 4$ . 9(b) shows the analytical results for  $\sigma_m/\sigma_0$  where

$$\sigma_m = \max(\sigma_{mf}, \sigma_{ms}, \sigma_{mm}).$$

698 Recall that  $\sigma_{mf}$ ,  $\sigma_{ms}$  and  $\sigma_{mm}$  are given by equations (3.17), (3.25) and (3.32), respectively.

699 As can be seen, the agreement between the numerical results and the asymptotic formulae is quite good except for  $(\mathcal{B}, \mathcal{N})$  belonging to a narrow band around  $\mathcal{N} = 3$  and  
 700  $\mathcal{B} \gtrsim f(\mathcal{N} = 3) = 1.6035$ . This can also be observed more quantitatively from figure 10  
 701 which shows  $\sigma_m/\varepsilon$  versus  $\mathcal{N}$  for some selected values of  $\mathcal{B} = 1$  (figure 10-a),  $\mathcal{B} = 2$  (figure  
 702 10-b),  $\mathcal{B} = 3$  (figure 10-c) and  $\mathcal{B} = 4$  (figure 10-d).

704 A closer examination of the regions of instability in the plane  $(\mu, \sigma + \varepsilon)$  for a given  $(\mathcal{B}, \mathcal{N})$

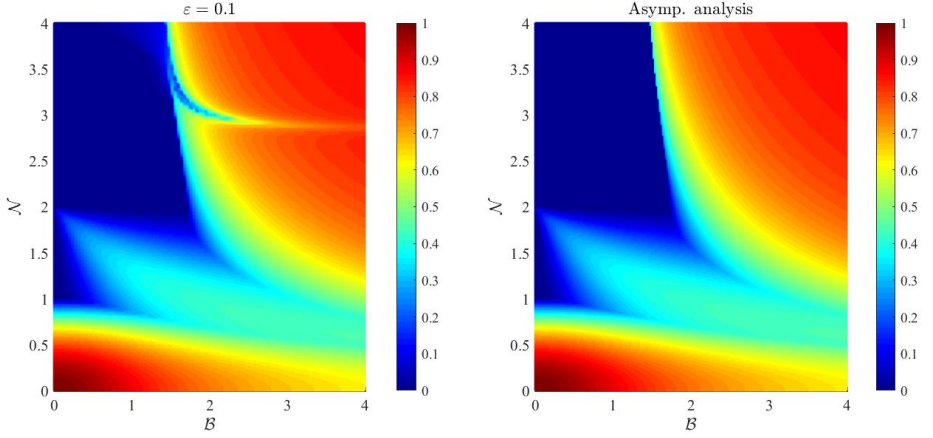


Figure 9

Magneto-gravity elliptic instabilities. Maximal growth rate of dominant instability normalised by  $\sigma_0 = 9/16$  plotted as a function of  $0 \leq \mathcal{B} \leq 4$  and  $0 \leq \mathcal{N} \leq 4$ . Left panel: numerical results for  $\varepsilon = 0.1$ . Right panel: asymptotic analysis results.

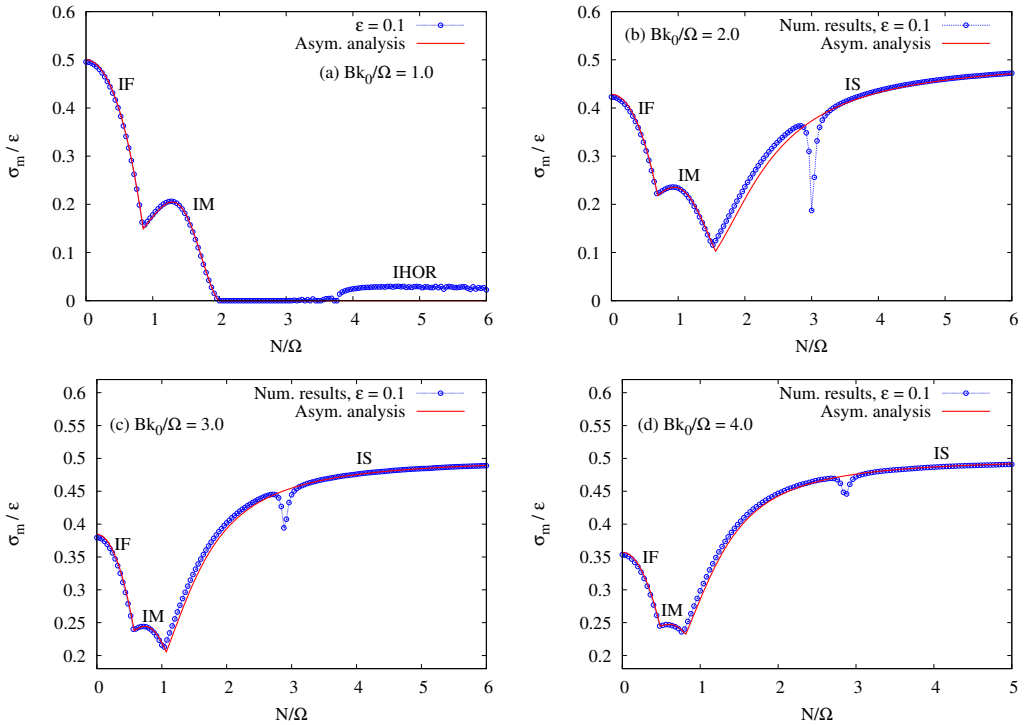


Figure 10

Magneto-gravity elliptic instabilities. Maximal growth rate of the dominant instability normalised by  $\varepsilon$  versus  $\mathcal{N}$  for selected values of  $\mathcal{B} = 1$  (figure 10-a),  $\mathcal{B} = 2$  (figure 10-b),  $\mathcal{B} = 3$  (figure 10-c) and  $\mathcal{B} = 4$  (figure 10-d). The figure compares the asymptotic formulae with the numerical results at  $\varepsilon = 0.1$ . The subharmonic instability resulting from a resonance between two fast (respectively, slow) modes is labelled by IF (respectively, IS), whereas that resulting from a resonance between a fast and a slow mode is labelled by IM. From figure 10-a, we observe that an instability related to higher-order resonances (IHOR) is present for  $\mathcal{N} > 3.7$ .



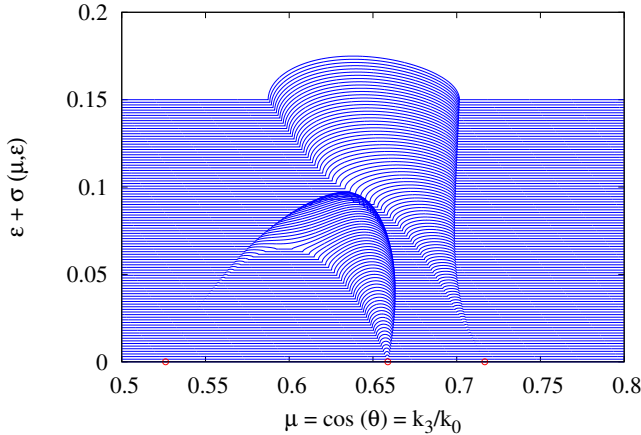


Figure 11

Magneto-gravity elliptic instabilities. The figure shows  $\sigma + \varepsilon$  versus  $\mu$  for  $\mathcal{N} = 3.1$  and  $\mathcal{B} = \sqrt{3}$ , and 100 values of  $\varepsilon$  regularly distributed in the interval  $0 \leq \varepsilon \leq 0.15$ . The subharmonic instability IS emanates from the point  $(0.6589, 0)$  and disappears beyond  $\varepsilon \approx 0.1$ . Before disappearing, the IS instability coalesces with the instability associated with a resonance of order  $n = 6$  between two slow modes which emanates from the point  $(0.5262, 0)$ . The region of instability emanating from the point  $(0.7168, 0)$  corresponds to the instability related to resonances of order  $n = 4$  between a fast mode and a slow mode.

705 belonging to the narrow band around  $\mathcal{N} = 3$  reveals that beyond  $\varepsilon \approx 0.1$  the subharmonic  
 706 instability resulting from the resonances between two slow modes disappears and it is the  
 707 instability related to resonances of order  $n = 4$  between a fast mode and a slow mode which  
 708 becomes dominant. This is illustrated by figure 11 which shows  $\sigma + \varepsilon$  versus  $\mu$  for  $\mathcal{N} = 3.1$  and  
 709  $\mathcal{B} = \sqrt{3}$ . It can be observed that, before disappearing, the subharmonic instability coalesces  
 710 with the instability related to the resonances of order  $n = 6$  between two slow modes. Recall  
 711 that for the identification of the different regions of instability we use equations (3.9) and  
 712 (3.10).

713 Similar conclusions are drawn from the analysis of the numerical results for  $0.1 < \varepsilon$  in  
 714 the sense that, for  $(\mathcal{B}, \mathcal{N})$  belonging to one of the domains I-VI, the dominant instability  
 715 corresponds to one of the subharmonic instabilities listed in section 3. As for the agreement  
 716 between the asymptotic formulae and the numerical results at  $\varepsilon > 0.1$ , it is not as satisfactory  
 717 as in the case of weak ellipticity ( $\varepsilon \lesssim 0.1$ ). Indeed, the difference between the numerical  
 718 results and the asymptotic formulae increases as  $\varepsilon$  increases especially for  $(\mathcal{B}, \mathcal{N})$  belonging  
 719 to the domains V and VI. This is illustrated by figure 12 that displays  $\sigma_m/\varepsilon$  versus  $\mathcal{N}$  for  
 720  $\mathcal{B} = 4$  and five values of  $\varepsilon = 0.1, 0.2, 0.3, 0.4$  and  $\varepsilon = 0.5$ .

721 We point out that the present numerical computations, as well as the asymptotic analysis,  
 722 do not detect any instabilities for  $2 < \mathcal{N} < 3$  and  $0 \leq \mathcal{B} \leq f(\mathcal{N} = 3) = 1.6035$ . As an  
 723 illustration, figure 13 shows the continuous variation of the maximal growth rate  $\sigma_m$  of the  
 724 dominant instability normalised by  $\sigma_0 = 9/16$  plotted as a function of  $0 \leq \mathcal{B} \leq 4$  and  
 725  $0 \leq \mathcal{N} \leq 4$  for  $\varepsilon = 0.5$  (left panel) and  $\varepsilon = 1$  (right panel).

#### 4.3. Accounting for diffusivity, in the simplest case

727 As indicated in the introduction, Singh and Mathur (2019) investigated the effects of  
 728 differential diffusion between momentum and density ( $Sc = \kappa/\nu$ ) in their local stability  
 729 analysis for an elliptical vortex with a uniform stable stratification along the vorticity axis.  
 730 They showed that in the case where  $Sc = \kappa/\nu = 1$  viscous effects are purely suppressive,

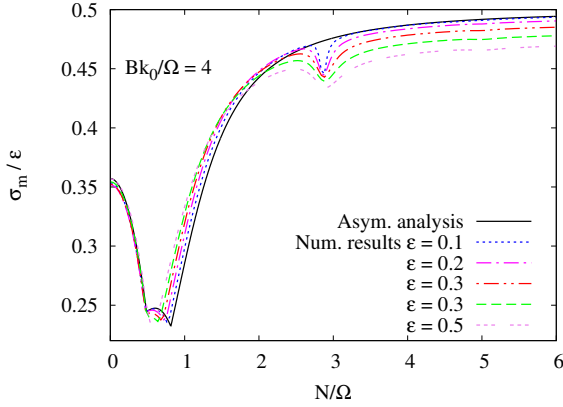


Figure 12

Magneto-gravity elliptic instabilities. Maximal growth rate of dominant instability normalised by  $\varepsilon$  versus  $\mathcal{N}$  for  $\varepsilon = 0.1, 0.2, 0.3, 0.4, 0.5$  and  $\mathcal{B} = 4$ .

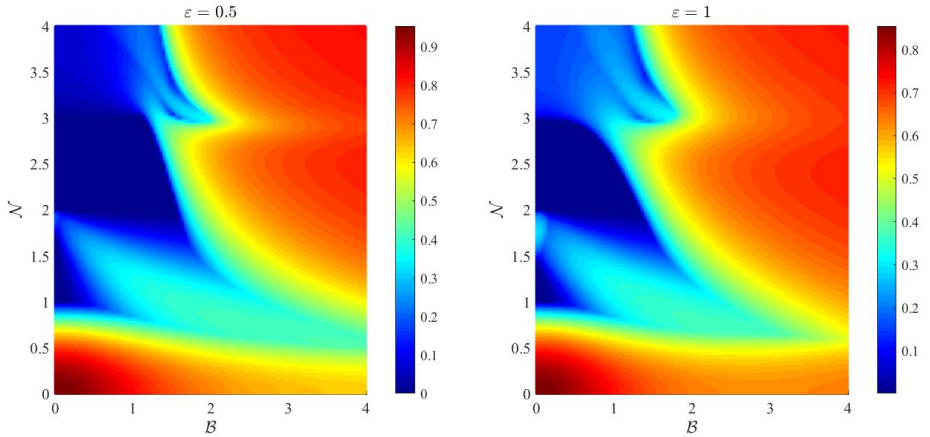


Figure 13

Magneto-gravity elliptic instabilities. Maximal growth rate of dominant instability normalised by  $\sigma_0 = 9/16$  plotted as a function of  $0 \leq \mathcal{B} \leq 4$  and  $0 \leq \mathcal{N} \leq 4$ . (a)  $\varepsilon = 0.5$ . (b)  $\varepsilon = 1$ .

731 whereas for sufficiently small  $Sc < 1$ , there is an oscillatory instability the signature of which  
732 is nevertheless present with zero growth rate in the inviscid limit.

733 The study of the effects of differential diffusion in the case of an elliptical vortex with  
734 a uniform stable stratification and a uniform magnetic field involves three dimensionless  
735 numbers, namely, the Reynolds number and the thermal and magnetic Prandtl numbers, in  
736 addition to the parameters  $\varepsilon$ ,  $\mathcal{B}$  and  $\mathcal{N}$ . This requires a detailed study and is beyond the scope  
737 of the present work. For instance, we consider the very special case where the diffusion  
738 coefficients are equal,  $\nu = \kappa = \eta$ .

739 In that case, the dispersion relation of the MIG waves is obtained by replacing  $\omega$  in equation  
740 (3.5) by  $(\omega - \nu k^2)$ , and the Fourier amplitudes of the velocity, magnetic field and buoyancy  
741 scalar perturbations may be associated with those in the inviscid limit  $\hat{\mathbf{u}}, \hat{\mathbf{b}}$  and  $\hat{\vartheta}$  by the  
742 substitution (Cambon *et al.* 1985; Landman & Saffman 1987)

$$743 \quad (\hat{\mathbf{u}}^{(v)}, \hat{\mathbf{b}}^{(v)}, \hat{\vartheta}^{(v)}) = (\hat{\mathbf{u}}, \hat{\mathbf{b}}, \hat{\vartheta}) \exp\left(-\nu \int_0^t k^2(s) ds\right). \quad (4.1)$$

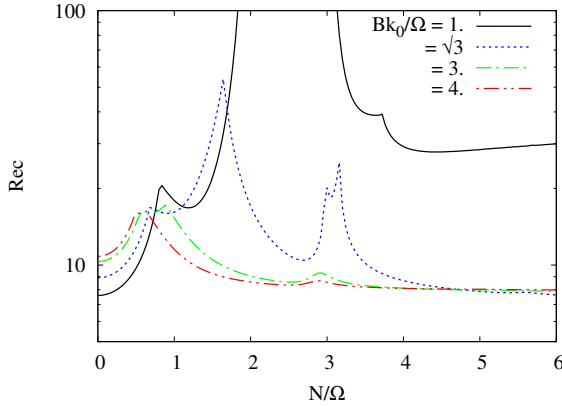


Figure 14

Case where the diffusivity coefficients (kinematic, magnetic and thermal) are equal. Variation of the critical Reynolds number  $Re_c$  versus  $\mathcal{N}$  for  $E = 1.5$  (therefore  $\varepsilon = 0.41667$ ) and  $\mathcal{B} = 1, \sqrt{3}, 3$  and  $\mathcal{B} = 4$ . Dominant instability can survive the effects of diffusion, provided  $Re > Re_c$ .

744 Accordingly, the maximal growth rate of the dominant instability, if attainable, is

$$745 \quad \sigma_m^{(v)} = \sigma_m - Re^{-1} k_0^2 L_0^2 \left( 1 + \frac{(E^2 - 1)(1 - \mu_m^2)}{2} \right) \quad (4.2)$$

746 where  $Re = \Omega L_0^2 / \nu$  is the Reynolds number,  $L_0$  is a characteristic length scale and  $\mu_m$  is the  
747 value of  $\mu$  where  $\sigma_m$  occurs. At  $L_0 k_0 \sim 1$ , the dominant instability survives the diffusive  
748 effects if  $Re > Re_c$ , where

$$749 \quad Re_c = \frac{2 + (E^2 - 1)(1 - \mu_m^2)}{2\sigma_m}. \quad (4.3)$$

750 Figure 14 shows the variation of  $Re_c$  versus  $\mathcal{N}$  for  $E = 1.5$  (so that  $\varepsilon = 0.41667$ ) and  
751  $\mathcal{B} = 1, \sqrt{3}, 3$  and  $\mathcal{B} = 4$ . It appears that in the case where  $\mathcal{B} \geq \sqrt{3}$ , the dominant instability  
752 survives the diffusion effects for  $Re_c \sim 50$  and  $(\mathcal{B}, \mathcal{N}) \in [\sqrt{3}, +\infty[ \times [0, +\infty[$ . Since there  
753 are no instabilities when  $2 < \mathcal{N} < 3$  and  $0 < \mathcal{B} < f(\mathcal{N}) = 1.6035$ , the critical Reynolds  
754 number  $Re_c$  takes large values for  $\mathcal{N}$  in the left (respectively, right) neighbourhood of  $\mathcal{N} = 2$   
755 (respectively,  $\mathcal{N} = 3$ ). This is the case for  $\mathcal{B} = 1$  that we observe in figure 14.

## 756 5. Concluding remarks

757 We have analysed here the joint influence of a stable stratification and an external uniform  
758 magnetic field on the stability of an unbounded flow with elliptical streamlines of a perfectly  
759 conducting fluid. Both stable stratification, via the mean buoyancy gradient, and mean  
760 magnetic field are in the axial direction. Such a simple model allows us to formulate the  
761 stability problem as a system of equations for disturbances in terms of Lagrangian Fourier  
762 modes which is universal for wavelengths of the perturbation sufficiently small with respect  
763 to the scale of variation of the mean velocity gradients. Moreover, it can similarly model  
764 localised patches of elliptical streamlines which often appear in geophysical and astrophysical  
765 flows. For example, an elliptical vortex patch embedded in the accretion disc can be created  
766 by the non-uniform average angular velocity profile in the disc. Indeed, some previous studies  
767 using the zonal asymptotic method of Lifschitz & Hameiri (1991) show that these localised  
768 patches of elliptical streamlines are unstable to short-wavelength instabilities regardless of what

769 type of flow surrounds (e.g., Lifschitz (1994); Sipp, Lauga & Jacquin (1999); Godeferd,  
770 Cambon & Leblanc (2001); Aravind, Dubos & Mathur (2022)).

771 The analysis presented in the present paper extends the study by Miyazaki & Fukumoto  
772 (1992) by including the effect of the (axial) magnetic field on the gravity-elliptic instability  
773 and the study by LZ04 by including the effect of an axial stratification on the magneto-  
774 elliptic instability. The stability analysis involves a non-homogeneous Floquet system with  
775 arbitrary value of the MIPS in its right-hand-side (equation (2.20)). For the purpose of  
776 the study of stability, this right-hand-side (equation (2.20) and equations (2.23) and (3.1))  
777 can be set to zero without lack of generality. Of course, the resulting homogeneous Floquet  
778 system (left-hand-side) already accounts for the invariance of the MIPS with parameters  
779  $(\mu, \varepsilon, k_0 B/\Omega, N/\Omega)$ . This is shown by equation (3.5) as well.

780 Because most of the instabilities appearing in this elliptical flow are due to the destabilising  
781 resonances, we have analysed in detail the resonant cases of the MIG waves propagating  
782 in flows with circular streamlines ( $\varepsilon = 0$ ). These resonant cases are of three types: the  
783 resonances between two fast modes, the resonances between a fast mode and slow mode and  
784 the resonances between two slow modes, where the last two types disappear in the absence of  
785 the unperturbed magnetic field. The asymptotic method at leading order in  $\varepsilon$  by LZ04 has been  
786 extended to determine the growth rates of the destabilising resonances of order  $n = 2$  (i.e. the  
787 subharmonic instability). It results from this analysis that the subharmonic instability operates  
788 for  $(k_0 B/\Omega, N/\Omega)$  belonging to the domain  $(]0, +\infty[ \times [0, 2]) \cup \left( [\sqrt{3} + \infty[ \times [2, +\infty[ \right) \cup \mathcal{D}_f$   
789 (see figure 2) where  $\mathcal{D}_f$  is defined by equation (3.12). Moreover, the present analysis reveals  
790 that the effects of stable (axial) stratification on the magneto-elliptical instability can be  
791 analyzed by distinguishing the two cases  $N \leq 2\Omega$  and  $N > 2\Omega$ .

792 *Case where  $0 < N \leq 2\Omega$ .* In that case, three subharmonic instabilities can exist: the  
793 IF (respectively, IS) instability results from resonances between two fast (slow) modes  
794 and the IM (M for mixed) instability results from resonances between a fast mode and a  
795 slow mode. For these three subharmonic instabilities, the  $N \rightarrow 0$  limit is, in fact, singular  
796 (discontinuous). The IF (respectively, IM) instability is completely suppressed by stable  
797 stratification when  $N/\Omega$  reaches 1, (respectively, 2), independently of the magnetic field  
798 strength. For  $0 < N/\Omega < 1$  (respectively,  $0 < N/\Omega < 2$ ) its maximal growth rate approaches  
799 zero for large  $k_0 B$ , whereas in the case without stratification, it approaches  $\varepsilon/4$ . As for the  
800 IS instability which only occurs for  $k_0 B/\Omega > \sqrt{3}$ , it is enhanced by the stable stratification  
801 because its maximal growth rate approaches  $\varepsilon/2$  for large  $k_0 B$  whereas without stratification  
802 it approaches  $\varepsilon/4$ .

803 *Case where  $N/\Omega > 2$ .* In that case, only the subharmonic instabilities resulting from  
804 resonances between two fast modes (IF<sup>+</sup>) or two slow modes (IS<sup>+</sup>) can occur. The IF<sup>+</sup>  
805 instability can only occur for  $2 < N/\Omega < +\infty$  and  $1 < f(N/\Omega) \leq B/\Omega < \sqrt{3}$  (i.e., the  
806 domain  $\mathcal{D}_f$ ). Its maximal growth rate, which approaches  $\varepsilon/2$  as  $k_0 B/\Omega \rightarrow +\infty$ , remains less  
807 than that of the IS<sup>+</sup> instability. On other words, for  $(k_0 B/\Omega, N/\Omega)$  belonging to the domain  
808  $\mathcal{D}_f$ , the IS<sup>+</sup> instability dominates the IF<sup>+</sup> instability (see figure 5). The IS<sup>+</sup> instability is also  
809 present for  $2 < N/\Omega < +\infty$  and  $\sqrt{3} < k_0 B/\Omega < +\infty$  with a maximal growth rate approaching  
810  $\varepsilon/2$  for large  $k_0 B$ . Note that the enhancement of the IS instability when the two backgrounds  
811 are simultaneously present is connected with a large exchange of energy between the kinetic  
812 and magnetic energies and between the kinetic and potential energies.

813 The analytical results were compared to the numerical results for several values of  $0 \leq$   
814  $\varepsilon \leq 1$ ,  $0 \leq \mathcal{B} \leq 4$  and  $0 \leq \mathcal{N} \leq 4$ . The comparison reveals that the subharmonic instability,  
815 if it exists, dominates the instabilities related to higher-order resonances ( $n = 4, 6, 8, \dots$ ).  
816 The agreement between the asymptotic formulae and the numerical results is quite good  
817 for small ellipticities ( $\varepsilon \lesssim 0.1$ ) (see figure 12). The numerical results also reveal that for a

818 narrow band around  $\mathcal{N} = 3$ , the dominant instability is rather that related to resonances of  
 819 order  $n = 4$  between a fast mode and a slow mode (see figure 11). Instabilities related to  
 820 higher-order resonances can occur for  $(\mathcal{B}, \mathcal{N}) \in [0, \sqrt{3}[\times]2, \infty[\backslash\mathcal{D}_f$  (e.g., see figure, 8).

821 The whole analysis developed in this study is essentially linear, and linearisation deserves  
 822 some discussion. On the one hand, it was clarified that a two-mode analysis is needed for the  
 823 destabilising resonances, in contrast with a single-mode analysis where the nonlinearity is  
 824 identically zero (Moffatt 2010; Craik & Criminale 1986). Other cases where the nonlinearity  
 825 is not explicit, but implicitly present, exist in the literature, especially in astrophysics, with  
 826 the regeneration of modes for bypass transition in accretion discs (e.g. Chagelishvili *et al.*  
 827 (2003)). Looking at the velocity field, linearisation cannot be justified by a small value of the  
 828 perturbed velocity field with respect to the base (mean) velocity field, which is extensional:  
 829 a ratio of time-scale is used instead in the so-called RDT as the linear ‘rapid’ limit: a typical  
 830 time-scale of the ‘turbulent’ velocity field is assumed to be large with respect to the time-scale  
 831 given by the (inverse of the magnitude of) the mean velocity gradients (e.g.  $\mathbf{A}$  in equation  
 832 (2.6a)). As suggested by an anonymous referee, some robustness of the linear solution results  
 833 from the particular mean flow configuration, where the periods of a fluid element moving  
 834 along different streamlines are the same. Accordingly, there is no growth of gradient, as a  
 835 source of nonlinearity, and thereby of wavenumber, across the streamlines direction.

836 The present analysis, which allowed us to map the domains of the  $(\mathcal{B}, \mathcal{N})$  space for  
 837 which the magneto-gravity-elliptic instability can operate, would serve to guide future DNS  
 838 for the study of the effects of nonlinearity on this instability. Note that, in the case of the  
 839 magneto-precessional instability, the regime of the saturation of this instability by nonlinear  
 840 interactions was identified. It corresponds to a saturation stage during which the total turbulent  
 841 energy (kinetic + magnetic), the production rate due to the base flow and the total dissipation  
 842 rate remain almost independent of time where the dissipation rate balances the production  
 843 rate (Salhi, Khelifi & Cambon 2020).

844 The question that can arise concerns the joint influence of Lorentz, Coriolis and buoyancy  
 845 forces on the elliptical instability. With the inclusion of the Coriolis force, in addition to  
 846 the Lorentz and buoyancy forces, the problem turns out to be more complex because the  
 847 resulting fourth four-component linear Floquet system becomes one with five parameters,  
 848 namely  $(\mu, \varepsilon, \mathcal{B}, \mathcal{N}, \Omega_c/\Omega)$ , ( $\Omega_c$  being the angular velocity of system rotation). For that we  
 849 preferred not to include, in this analysis, the effect of the Coriolis force.

850 As a useful extension of our present study, more complex but with a similar analysis, an  
 851 additional Coriolis force can be introduced. Keeping the same effects of stratified MHD, the  
 852 problem will include the angular velocity  $\Omega_c$  of the system rotation in addition to the basic  
 853 angular velocity  $\Omega$ . Moreover, for anticyclonic rotation (i.e.  $\Omega_c \leq -\Gamma/2 = -\Omega(E + E^{-1})/4$ ),  
 854 the horizontal instability is dominant (Bajer & Mizerski 2013)). Indeed, when the wave  
 855 vector is axial (here, the vectors  $\Omega_c$ ,  $\mathbf{B}$  and  $\nabla_\rho$  are also axial) there is no effect of the  
 856 buoyancy force (in the linear regime) since the frequency of gravity waves is zero ( $\omega_g = 0$ ).  
 857 In that case, the maximal growth rate of the horizontal instability, which is not of resonant  
 858 nature, is about  $\sigma_m/\varepsilon = 1$  for  $(k_3 B)^2 = -\Omega^2(1 + 2\Omega_c/\Omega)$  in the limit of small  $\varepsilon$  (so that,  
 859  $\Gamma = \Omega(1 + O(\varepsilon^2))$ ). The study of the effect of cyclonic rotation on the magneto-gravity-elliptic  
 860 instability, as well as the study of the joint influence of a stable stratification and unperturbed  
 861 magnetic field on the precessional instability, are the subject of future studies.

## 862 Appendix A. Asymptotic analysis at leading order in $\varepsilon$ of the Floquet system (2.23)

863 In this appendix, we extend the asymptotic method of LZ04 to determine, at leading order  
 864 in  $\varepsilon$ , the maximal growth rate of the solution of the four-component Floquet system (2.23),

865  $d_\tau \hat{\mathbf{c}} = \mathbf{D} \cdot \hat{\mathbf{c}}$ . Recall that  $\Phi(\tau, \varepsilon, \mu, \mathcal{B}, \mathcal{N})$  denotes the fundamental matrix solution,

$$866 \quad d_\tau \Phi = \mathbf{D} \cdot \Phi, \quad \Phi(\tau = 0) = \mathbf{I}_4 \quad (\text{A } 1)$$

867 and  $\mathbf{M} = \Phi(2\pi, \varepsilon, \mu, \mathcal{B}, \mathcal{N})$  denotes the Floquet multiplier matrix where its determinant is  
868 unity (see the end of section 2.3.). It follows that whenever  $\lambda$  is an eigenvalue of  $\mathbf{M}$ , so also  
869 are its inverse  $\lambda^{-1}$  and its complex conjugate  $\lambda^*$ . We denote by

$$870 \quad p(\lambda, \varepsilon) = |\mathbf{M} - \lambda \mathbf{I}_4| \quad (\text{A } 2)$$

871 the characteristic polynomial of the characteristic polynomial of the Floquet multiplier matrix  
872  $\mathbf{M}$  and by  $\Lambda_1, \Lambda_2, \Lambda_3$  and  $\Lambda_4$  its roots. A necessary condition for stability is that each root lie  
873 on the unit circle (see LZ04).

#### 874 A.1. *Expansion in Taylor series of the Floquet multiplier matrix*

875 We expand the Floquet multiplier matrix  $\mathbf{M}(\varepsilon, \mu, \mathcal{B}, \mathcal{N})$  in Taylor series in the neighbourhood  
876 of  $(\varepsilon, \mu) = (0, \mu_0)$ , holding  $(\mathcal{B}, \mathcal{N})$  constant,

$$877 \quad \mathbf{M} = \mathbf{M}_0(\mu_0, 0) + \varepsilon \mathbf{M}_\varepsilon(\mu_0, 0) + (\mu - \mu_0) \mathbf{M}_\mu(\mu_0, 0) + \dots \quad (\text{A } 3)$$

878 where  $\mathbf{M}_\varepsilon = (\partial \mathbf{M} / \partial \varepsilon)$ ,  $\mathbf{M}_\mu = (\partial \mathbf{M} / \partial \mu)$  and the dots indicate higher-order terms in  $\varepsilon$  and  
879  $\mu - \mu_0$ . In general, at sufficiently small  $\varepsilon$ , the region in the the  $(\varepsilon, \mu)$  plane where instability  
880 occurs is typically a wedge with apex at a point  $(\varepsilon, \mu) = (0, \mu_0)$  and boundaries

$$881 \quad \mu = \mu_0 + \gamma_\pm \varepsilon \quad (\text{A } 4)$$

882 where the slopes  $\gamma_+$  and  $\gamma_-$  are to be found. The instability (if it exists) has a bandwidth  
883  $(\gamma_+ - \gamma_-) \varepsilon$  : that is, for given  $\varepsilon$ ,  $\mathcal{B}$  and  $\mathcal{N}$ , the length of the  $\mu$ -interval for which the  
884 wavenumbers are unstable. Therefore, equation (A 3) can be rewritten as

$$885 \quad \mathbf{M} = \mathbf{M}_0 + \varepsilon \mathbf{M}_1 + O(\varepsilon^2) \quad (\text{A } 5a)$$

$$886 \quad \mathbf{M}_1 = \mathbf{M}_\varepsilon + \gamma \mathbf{M}_\mu. \quad (\text{A } 5b)$$

888 Accordingly, we no longer need the designation  $\mu_0$  and, hereinafter, use the symbol  $\mu$  in its  
889 place.

890 To determine matrices  $\mathbf{M}_0$ ,  $\mathbf{M}_\varepsilon$  and  $\mathbf{M}_\mu$ , we expand, for a given  $\tau \in [0, 2\pi]$ ,  $\Phi$  and  $\mathbf{D}$ ,

$$891 \quad \Phi(\tau, \varepsilon) = \Phi_0(\tau, \mu, 0) + \varepsilon \Phi_1(\tau, \mu, 0) + O(\varepsilon^2), \quad (\text{A } 6a)$$

$$892 \quad \mathbf{D}(\tau, \varepsilon) = \mathbf{D}_0 + \varepsilon \mathbf{D}_\varepsilon(\tau, 0) + O(\varepsilon^2) \quad (\text{A } 6b)$$

where  $\Phi_0(\tau = 0) = \mathbf{I}_4$  and  $\Phi_1(\tau = 0) = \mathbf{0}$ . Substituting (A 6) into (A 1), we obtain

$$d_\tau \Phi_0 = \mathbf{D}_0 \cdot \Phi_0, \quad d_\tau \Phi_1 = \mathbf{D}_0 \cdot \Phi_1 + \mathbf{D}_\varepsilon \cdot \Phi_0,$$

894 with solution  $\Phi_0(\tau) = e^{\tau \mathbf{D}_0}$  and

$$895 \quad \Phi_1(\tau) = \Phi_0(\tau) \cdot \left( \int_0^\tau \Phi_0^{-1}(s) \cdot \mathbf{D}_\varepsilon(s) \cdot \Phi_0(s) ds \right). \quad (\text{A } 7)$$

896 Because the characteristic polynomial  $p(\lambda, \varepsilon)$  is the same in any coordinate system and the  
897 four eigenvalues of the matrix  $\mathbf{D}_0$ , given by equation (3.5) (repeated here for the sake of

898 clarity) are distinct

$$899 \quad \sigma_1 = -\sigma_2 = -\frac{i}{\sqrt{2}} \sqrt{(4 + 2\mathcal{B}^2 - \mathcal{N}^2) \mu^2 + \mathcal{N}^2 + \sqrt{[(4 - \mathcal{N}^2) \mu^2 + \mathcal{N}^2]^2 + 16\mathcal{B}^2 \mu^4}} \quad (\text{A } 8a)$$

$$900 \quad \sigma_3 = -\sigma_4 = -\frac{i}{\sqrt{2}} \sqrt{(4 + 2\mathcal{B}^2 - \mathcal{N}^2) \mu^2 + \mathcal{N}^2 - \sqrt{[(4 - \mathcal{N}^2) \mu^2 + \mathcal{N}^2]^2 + 16\mathcal{B}^2 \mu^4}} \quad (\text{A } 8b)$$

902 as long as  $\mathcal{B} \neq 0$  and  $0 < \mu^2 < 1$ , we transform the solution in the base diagonalising  $\mathbf{D}_0$ ,

$$903 \quad \tilde{\mathbf{D}}_0 = \mathbf{T}^{-1} \cdot \mathbf{D}_0 \cdot \mathbf{T} = \text{diag}(\sigma_1, -\sigma_1, \sigma_3, -\sigma_3). \quad (\text{A } 9)$$

904 Here, the columns of  $\mathbf{T}$  are the eigenvectors of  $\mathbf{D}_0$ ,

$$905 \quad \mathbf{T} = \begin{pmatrix} \sigma_1 & -\sigma_1 & \sigma_3 & -\sigma_3 \\ -\frac{1}{2}(\sigma_1^2 + m^2) & -\frac{1}{2}(\sigma_1^2 + m^2) & -\frac{1}{2}(\sigma_3^2 + m^2) & -\frac{1}{2}(\sigma_3^2 + m^2) \\ im & im & im & im \\ -\frac{i}{2} \frac{m}{\sigma_1} (\sigma_1^2 + m^2) & \frac{i}{2} \frac{m}{\sigma_1} (\sigma_1^2 + m^2) & -\frac{i}{2} \frac{m}{\sigma_3} (\sigma_3^2 + m^2) & \frac{i}{2} \frac{m}{\sigma_3} (\sigma_3^2 + m^2) \end{pmatrix} \quad (\text{A } 10)$$

$$906 \quad \mathbf{T}^{-1} = \frac{1}{(\sigma_1^2 - \sigma_3^2)} \begin{pmatrix} \frac{1}{2} \frac{\sigma_1}{m^2} (\sigma_3^2 + m^2) & -1 & \frac{i}{2m} (\sigma_3^2 + m^2) & -\frac{i\sigma_1 \sigma_3^2}{m^3} \\ -\frac{1}{2} \frac{\sigma_1}{m^2} (\sigma_3^2 + m^2) & -1 & \frac{i}{2m} (\sigma_3^2 + m^2) & \frac{i\sigma_1 \sigma_3^2}{m^3} \\ -\frac{1}{2} \frac{\sigma_3}{m^2} (\sigma_1^2 + m^2) & 1 & -\frac{i}{2m} (\sigma_1^2 + m^2) & \frac{i\sigma_3 \sigma_1^2}{m^3} \\ \frac{1}{2} \frac{\sigma_3}{m^2} (\sigma_1^2 + m^2) & 1 & -\frac{i}{2m} (\sigma_1^2 + m^2) & -\frac{i\sigma_3 \sigma_1^2}{m^3} \end{pmatrix}, \quad (\text{A } 11)$$

908 where  $m = \mathcal{B}\mu$ . Therefore, in the base diagonalising  $\mathbf{D}_0$ ,  $\tilde{\mathbf{M}}_0$  and  $\tilde{\mathbf{M}}_\varepsilon$  take the form

$$909 \quad \tilde{\mathbf{M}}_0 = \mathbf{T}^{-1} \cdot \mathbf{M}_0 \cdot \mathbf{T} = \mathbf{diag} \left( e^{2\pi\sigma_1}, e^{-2\pi\sigma_1}, e^{2\pi\sigma_3}, e^{-2\pi\sigma_3} \right) = \mathbf{diag}(\lambda_1, \lambda_2, \lambda_3, \lambda_4), \quad (\text{A } 12a)$$

$$910 \quad \tilde{\mathbf{M}}_\varepsilon = \mathbf{T}^{-1} \cdot \mathbf{M}_\varepsilon \cdot \mathbf{T} = \tilde{\mathbf{M}}_0 \cdot \tilde{\mathbf{J}}, \quad (\text{A } 12b)$$

$$911 \quad \tilde{J}_{ij} = \left( \mathbf{T}^{-1} \right)_{im} T_{lj} \int_0^{2\pi} e^{(\sigma_j - \sigma_i)\tau} (\mathbf{D}_\varepsilon)_{ml}(\tau) d\tau. \quad (\text{A } 12c)$$

913 To complete the construction of the matrix  $\tilde{\mathbf{M}}_1$ , which appears in (A 5), we need the derivative  
914 of  $\tilde{\mathbf{M}}_0(\mu) = \tilde{\mathbf{M}}(\mu, 0)$  with respect to  $\mu$ ,

$$915 \quad \gamma \tilde{\mathbf{M}}_\mu = \gamma \frac{\partial \tilde{\mathbf{M}}_0}{\partial \mu} = \frac{2i\pi\gamma}{\Omega} \mathbf{diag} \left( \frac{\partial \omega_1}{\partial \mu} \lambda_1, \frac{\partial \omega_2}{\partial \mu} \lambda_2, \frac{\partial \omega_3}{\partial \mu} \lambda_3, \frac{\partial \omega_4}{\partial \mu} \lambda_4 \right). \quad (\text{A } 13)$$

## 916 A.2. Expansion of the characteristic polynomial

917 We expand the characteristic polynomial in Taylor series around  $\varepsilon = 0$  to second order in  $\varepsilon$ ,

$$918 \quad p(\lambda, \varepsilon) = p_0(\lambda) + p_1(\lambda)\varepsilon + p_2(\lambda)\varepsilon^2 + \mathcal{O}(\varepsilon^3), \quad (\text{A } 14)$$

where  $p_0(\lambda)$  is the characteristic polynomial of  $\mathbf{M}_0$  with roots  $\lambda_1 = e^{2\pi\sigma_1}$ ,  $\lambda_2 = e^{-2\pi\sigma_1}$ ,  $\lambda_3 = e^{2\pi\sigma_3}$  and  $\lambda_4 = e^{-2\pi\sigma_3}$ . Although  $\sigma_1, \sigma_2, \sigma_3$  and  $\sigma_4$  are distinct, it is possible for the multipliers  $\lambda_j$  ( $j = 1, 2, 3, 4$ ) to be repeated: if  $\sigma_j - \sigma_m = i\ell$  for an integer  $\ell \neq 0$ , then  $\lambda_j = \lambda_m$ . As shown by LZ04, a necessary condition for the onset of instability is that there be a double (or higher) root of the characteristic equation. As we only consider the case in which the eigenvalues are multiplicity 2, the Puiseux expansion takes the form

$$\Lambda_1 = \lambda_1 + \varepsilon^{\frac{1}{2}} \beta_{\frac{1}{2}} + \varepsilon \beta_1 + \mathcal{O}(\varepsilon^{\frac{3}{2}}),$$



919 where, for definiteness, we have assumed that  $\lambda_1 = \lambda_2$ . It can be shown, however, that  
 920  $\beta_{\frac{1}{2}} = 0$ , in this case, and then the leading-order correction to the eigenvalue,  $\beta_1 \neq 0$ , can be  
 921 established from a quadratic equation

$$922 \quad \frac{1}{2} \left[ \frac{d^2 p_0}{d\lambda^2}(\lambda_1) \right] \beta_1^2 + \left[ \frac{dp_1}{d\lambda}(\lambda_1) \right] \beta_1 + p_2(\lambda_1) = 0. \quad (\text{A } 15)$$

923 By the use of the formulae for the derivatives of the characteristic polynomial with respect  
 924 to parameter  $\varepsilon$ , derived by LZ04 (see their appendix B), we obtain

$$925 \quad \frac{d^2 p_0}{d\lambda^2}(\lambda_1) = 2(\lambda_3 - \lambda_1)(\lambda_4 - \lambda_1) \quad (\text{A } 16a)$$

$$926 \quad p_1(\lambda_1) = \sum_{j=1}^4 (\tilde{\mathbf{M}}_1)_{jj} \prod_{\ell \neq j} (\lambda_\ell - \lambda), \quad (\text{A } 16b)$$

$$927 \quad \frac{dp_1}{d\lambda}(\lambda_1) = [(\tilde{\mathbf{M}}_1)_{11} + (\tilde{\mathbf{M}}_1)_{22}] (\lambda_3 - \lambda_1)(\lambda_4 - \lambda_1), \quad (\text{A } 16c)$$

$$928 \quad p_2(\lambda_1) = \begin{vmatrix} (\tilde{\mathbf{M}}_1)_{11} & (\tilde{\mathbf{M}}_1)_{12} \\ (\tilde{\mathbf{M}}_1)_{21} & (\tilde{\mathbf{M}}_1)_{22} \end{vmatrix} (\lambda_3 - \lambda_1)(\lambda_4 - \lambda_1). \quad (\text{A } 16d)$$

930 Going back to the general case of  $\lambda_j = \lambda_m$ , the quadratic equation (A 15), with the aid  
 931 of (A 5b), (A 12) and (A 16) can easily be transformed to an equation for the coefficient  
 932  $\alpha = \beta/\lambda_j$ ,

$$\alpha^2 - \left( \tilde{J}_{jj} + \tilde{J}_{mm} + \frac{2i\pi\gamma}{\Omega} \left( \frac{\partial\omega_j}{\partial\mu} + \frac{\partial\omega_m}{\partial\mu} \right) \right) \alpha + \begin{vmatrix} \tilde{J}_{jj} + \frac{2i\pi\gamma}{\Omega} \frac{\partial\omega_j}{\partial\mu} & \tilde{J}_{jm} \\ \tilde{J}_{mj} & \tilde{J}_{mm} + \frac{2i\pi\gamma}{\Omega} \frac{\partial\omega_m}{\partial\mu} \end{vmatrix} = 0. \quad (\text{A } 17)$$

933

934 Therefore, either  $\alpha$  is pure imaginary and we infer stability (to leading order in  $\varepsilon$ ), or  $\text{Re } \alpha \neq 0$   
 935 and we infer instability (see the proposition 2 in LZ04).

### 936 A.3. Maximal growth rates of subharmonic instabilities

937 The solutions of the quadratic equation (A 17) take the form,

$$938 \quad \alpha = \frac{1}{2} \left[ \tilde{J}_{jj} + \tilde{J}_{mm} + \frac{2i\pi\gamma}{\Omega} \left( \frac{\partial\omega_j}{\partial\mu} + \frac{\partial\omega_m}{\partial\mu} \right) \right] \pm \frac{1}{2} \sqrt{D} \quad (\text{A } 18)$$

939 where the expression for  $D$  can be put in the form

$$940 \quad D = - \left| \tilde{J}_{jj} - \tilde{J}_{mm} + \frac{2i\pi\gamma}{\Omega} \left( \frac{\partial\omega_j}{\partial\mu} - \frac{\partial\omega_m}{\partial\mu} \right) \right|^2 + 4\tilde{J}_{jm}\tilde{J}_{mj} \quad (\text{A } 19)$$

because all the diagonal elements of the matrix  $\tilde{\mathbf{J}}$  are pure-imaginary numbers (see below).  
 The discriminant  $D$  must be greater than zero in order to have instability, so that

$$4\tilde{J}_{jm}\tilde{J}_{mj} > \left| \tilde{J}_{jj} - \tilde{J}_{mm} + \frac{2i\pi\gamma}{\Omega} \left( \frac{\partial\omega_j}{\partial\mu} - \frac{\partial\omega_m}{\partial\mu} \right) \right|^2 > 0.$$

941 Now the maximal growth rate, which in this case is achieved for

$$942 \quad \gamma = \frac{i\Omega (\tilde{J}_{jj} - \tilde{J}_{mm})}{2\pi \left( \frac{\partial\omega_j}{\partial\mu} - \frac{\partial\omega_m}{\partial\mu} \right)} \in \mathbb{R} \quad (\text{A } 20)$$



943 is

$$944 \quad \sigma_{max} = \frac{\varepsilon}{2\pi} (\text{Re } \alpha)_{max} = \frac{\varepsilon}{2\pi} \sqrt{\tilde{J}_{jm}\tilde{J}_{mj}} \quad (\text{with } j \neq m). \quad (\text{A } 21)$$

945 We now show that the diagonal elements of the matrix  $\tilde{\mathbf{J}}$  are pure-imaginary numbers.

946 From Equation (2.21) giving the matrix  $\mathbf{D}$ , we deduce  $\mathbf{D}_\varepsilon$ , where its non-zero elements  
947 are

$$948 \quad (\mathbf{D}_\varepsilon)_{11} = i \left(1 - \mu^2\right) \left(e^{2i\tau} - e^{-2i\tau}\right) \quad (\text{A } 22a)$$

$$949 \quad (\mathbf{D}_\varepsilon)_{14} = \frac{\mathcal{N}^2 (1 - \mu^2)}{2\mathcal{B} \mu} \left(e^{2i\tau} - e^{-2i\tau}\right) \quad (\text{A } 22b)$$

$$950 \quad (\mathbf{D}_\varepsilon)_{21} = \mu^2 \left(1 - \mu^2\right) \left(e^{2i\tau} + e^{-2i\tau} - 2\right) \quad (\text{A } 22c)$$

$$951 \quad (\mathbf{D}_\varepsilon)_{24} = -i \frac{\mathcal{N}^2}{2\mathcal{B}} \mu \left(1 - \mu^2\right) \left(e^{2i\tau} + e^{-2i\tau} - 2\right) \quad (\text{A } 22d)$$

952 Substituting the above expressions into (A 12c) and using (A 10) and (A 11) we obtain

$$954 \quad \tilde{J}_{jj} = \left(\mathbf{T}^{-1}\right)_{j2} \left(T_{1j} \int_0^{2\pi} (\mathbf{D}_\varepsilon)_{21} d\tau + T_{4j} \int_0^{2\pi} (\mathbf{D}_\varepsilon)_{24} d\tau\right) \quad (\text{A } 23a)$$

$$955 \quad \tilde{J}_{11} = -\tilde{J}_{22} = i\pi\mu^2 \left(1 - \mu^2\right) \frac{(4 - \mathcal{N}^2) \omega_1^2 + \mathcal{N}^2 \mathcal{B}^2 \mu^2}{\omega_1 (\omega_3^2 - \omega_1^2)} \quad (\text{A } 23b)$$

$$956 \quad \tilde{J}_{33} = -\tilde{J}_{44} = -i\pi\mu^2 \left(1 - \mu^2\right) \frac{(4 - \mathcal{N}^2) \omega_3^2 + \mathcal{N}^2 \mathcal{B}^2 \mu^2}{\omega_3 (\omega_3^2 - \omega_1^2)}, \quad (\text{A } 23c)$$

957

958 in which, as well as throughout the remainder of this appendix, the frequencies  $\omega_1$  and  
959  $\omega_3$  are normalised by  $\Omega$ . Equation (A 23) proves that the diagonal elements of the matrix  
960  $\tilde{\mathbf{J}}$  are pure-imaginary numbers. This implies that the slopes  $\gamma_\pm$ , which are solutions of  
961 the equation  $\text{Re}(\alpha) = 0$ , are also solutions of the equation  $\text{Re}(\sqrt{D}) = 0$ . The expression  
962 of  $D$  given by (A 19) involves the term  $(\partial_\mu \omega_j - \partial_\mu \omega_m)$ . However the dependence of the  
963 frequencies  $\omega_j$  and  $\omega_m$  on the variable  $\mu$  is not linear which increases the complexity of  
964 an analytical development in the resolution of  $\text{Re}(\sqrt{D}) = 0$ . It appears more convenient  
965 to perform analytically the derivatives  $\partial_\mu \omega_j$  and  $\partial_\mu \omega_m$ , and to resolve numerically the  
966 equation  $\text{Re}(\sqrt{D}) = 0$ .

967

968 We now calculate the maximal growth rates associated with the three unstable cases,  
969 namely the fast-fast (case 1), slow-slow (case 2) and fast-slow (case 3) destabilising  
970 resonances.

### 971 A.3.1. Case 1

972 The frequencies  $\omega_1$  and  $\omega_2 = -\omega_1$  given by (3.4a) correspond to fast modes and a resonance  
973 (or order  $n = 2$ ) between them is characterised by  $\omega_1 - \omega_2 = 2$ , so

$$974 \quad \omega_1 = -\omega_2 = 1 \quad \text{or} \quad \sigma_1 = -\sigma_2 = i. \quad (\text{A } 24)$$

975 The maximal growth rate of the subharmonic instability IF, denoted by  $\sigma_{mf}$ , is described by  
976 (A 21) which, in this case, reduces to

$$977 \quad \sigma_{mf} = \frac{\varepsilon}{2\pi} (\text{Re } \alpha)_{max} = \frac{\varepsilon}{2\pi} \sqrt{\tilde{J}_{12}\tilde{J}_{21}} \quad (\text{A } 25)$$

978 with

$$979 \quad \tilde{J}_{12} = \left(\mathbf{T}^{-1}\right)_{1m} T_{n2} \int_0^{2\pi} e^{-2i\tau} (\mathbf{D}_\varepsilon)_{mn} d\tau = \left(\mathbf{T}^{-1}\right)_{1m} T_{n2} H_{mn}^+ \quad (\text{A } 26a)$$

$$980 \quad \tilde{J}_{21} = \left(\mathbf{T}^{-1}\right)_{2m} T_{n1} \int_0^{2\pi} e^{+2i\tau} (\mathbf{D}_\varepsilon)_{mn} d\tau = \left(\mathbf{T}^{-1}\right)_{2m} T_{n1} H_{mn}^- \quad (\text{A } 26b)$$

982 where, given (A 22), the non-zero elements  $H_{mn}^+$  and  $H_{mn}^-$  take the form

$$983 \quad H_{11}^+ = -H_{11}^- = 2i\pi(1 - \mu^2) \quad (\text{A } 27a)$$

$$984 \quad H_{14}^+ = -H_{14}^- = \pi \frac{\mathcal{N}^2 (1 - \mu^2)}{\mathcal{B} \mu} \quad (\text{A } 27b)$$

$$985 \quad H_{21}^+ = H_{21}^- = 2\pi\mu^2(1 - \mu^2) \quad (\text{A } 27c)$$

$$986 \quad H_{24}^+ = H_{24}^- = -i\pi \frac{\mathcal{N}^2}{\mathcal{B}} \mu(1 - \mu^2). \quad (\text{A } 27d)$$

988 With the aid of (A 10) and (A 11) one easily shows that  $\tilde{J}_{21} = -\tilde{J}_{12}$ . Now back to determining  
989 the element  $\tilde{J}_{12}$

$$990 \quad \tilde{J}_{12} = \left(\mathbf{T}^{-1}\right)_{11} (H_{11}^+ T_{12} + H_{14}^+ T_{42}) + \left(\mathbf{T}^{-1}\right)_{12} (H_{21}^+ T_{12} + H_{24}^+ T_{42}). \quad (\text{A } 28)$$

991 The substitution of  $\mathbf{T}_{ij}^{-1}$ ,  $H_{ij}^+$  and  $T_{ij}$  by their expressions respectively given by (A 11), (A 27)  
992 and (A 10) into (A 28) leads to

$$993 \quad \tilde{J}_{12} = -\tilde{J}_{21} = -\frac{i\pi}{4} \frac{(1 - \mu^2)}{(1 - \omega_3^2)} \left(4 - \mathcal{N}^2 + \mathcal{B}^2 \mathcal{N}^2 \mu^2\right) \left(1 + 2\mu^2 - \frac{\omega_3^2}{\mathcal{B}^2 \mu^2}\right). \quad (\text{A } 29)$$

994 From equations (3.4a) and (3.4b) giving the expression of the frequencies  $\omega_1$  and  $\omega_3$ , we  
995 deduce that

$$996 \quad \omega_1^2 + \omega_3^2 = 1 + \omega_3^2 = \left(4 + 2\mathcal{B}^2 - \mathcal{N}^2\right) \mu^2 + \mathcal{N}^2 \quad (\text{A } 30)$$

997 because  $\omega_1 = 1$  in case 1. Moreover, with the aid of the resonance condition (3.9), we deduce  
998 the equality

$$999 \quad \omega_3^2 = \left(4 + 2\mathcal{B}^2 - \mathcal{N}^2\right) \mu^2 + \mathcal{N}^2 - 1 = \mathcal{B}^2 \mu^2 \left[\left(\mathcal{B}^2 - \mathcal{N}^2\right) \mu^2 + 1\right]. \quad (\text{A } 31)$$

1000 Accordingly, the substitution of (A 31) into (A 29) leads to

$$1001 \quad \tilde{J}_{12} = -\tilde{J}_{21} = -\frac{i\pi}{4} \left(3 - \mathcal{B}^2 \mu^2\right) \left(1 + \mathcal{B}^2 \mu^2\right) \frac{\left[\left(\mathcal{N}^2 - \mathcal{B}^2 + 2\right) \mu^2 + \left(1 - \mathcal{N}^2\right)\right]}{\left[\left(\mathcal{N}^2 - 2\mathcal{B}^2 - 4\right) \mu^2 + \left(2 - \mathcal{N}^2\right)\right]}. \quad (\text{A } 32)$$

Hence, we obtain the expression of

$$\frac{\sigma_{mf}}{\varepsilon} = \frac{1}{2\pi} (\text{Re } \alpha)_{max} = \frac{1}{2\pi} \sqrt{\tilde{J}_{12} \tilde{J}_{21}} = \sqrt{-\left(\tilde{J}_{12}\right)^2} \geq 0$$

1002 given by (3.17) in which the parameter  $\mu$  is given by (3.14).

### 1003 A.3.2. Case 2

1004 The frequencies  $\omega_3$  and  $\omega_4 = -\omega_3$  given by (3.4b) correspond to slow modes and a resonance  
1005 (or order  $n = 2$ ) between them is characterised by  $\omega_3 - \omega_4 = 2$ , so

$$1006 \quad \omega_3 = -\omega_4 = 1 \quad \text{or} \quad \sigma_3 = -\sigma_4 = i. \quad (\text{A } 33)$$

1007 The maximal growth rate of the subharmonic instability IS, denoted by  $\sigma_{ms}$ , is then described  
1008 by (A 21) which, in this case, reduces to

$$1009 \quad \sigma_{ms} = \frac{\varepsilon}{2\pi} (\operatorname{Re} \alpha)_{max} = \frac{\varepsilon}{2\pi} \sqrt{\tilde{J}_{34}\tilde{J}_{43}}. \quad (\text{A } 34)$$

1010 With the aid of (A 10) and (A 11) we show that  $\tilde{J}_{43} = -\tilde{J}_{34}$ . The determination of the element

$$1011 \quad \tilde{J}_{34} = \left(\mathbf{T}^{-1}\right)_{31} (H_{11}^+ T_{12} + H_{14}^+ T_{44}) + \left(\mathbf{T}^{-1}\right)_{32} (H_{21}^+ T_{14} + H_{24}^+ T_{44}) \quad (\text{A } 35)$$

1012 is similar to that of  $\tilde{J}_{12}$  since if we perform the permutation  $\sigma_1 \leftrightarrow \sigma_3$  in the expression of  
1013  $(\mathbf{T}^{-1})_{11}$ ,  $(\mathbf{T}^{-1})_{12}$ ,  $T_{12}$  and  $T_{42}$  in (A 10) and (A 11) we obtain the expression of  $(\mathbf{T}^{-1})_{31}$ ,  
1014  $(\mathbf{T}^{-1})_{32}$ ,  $T_{14}$  and  $T_{44}$ , and, hence,

$$1015 \quad \tilde{J}_{34} = -\tilde{J}_{43} = -\frac{i\pi}{4} \frac{(1 - \mu^2)}{(1 - \omega_1^2)} \left(4 - \mathcal{N}^2 + \mathcal{B}^2 \mathcal{N}^2 \mu^2\right) \left(1 + 2\mu^2 - \frac{\omega_1^2}{\mathcal{B}^2 \mu^2}\right), \quad (\text{A } 36)$$

1016 where

$$1017 \quad \omega_1^2 = \left(4 + 2\mathcal{B}^2 - \mathcal{N}^2\right) \mu^2 + \mathcal{N}^2 - 1 = \mathcal{B}^2 \mu^2 \left[\left(\mathcal{B}^2 - \mathcal{N}^2\right) \mu^2 + 1\right]. \quad (\text{A } 37)$$

1018 Thus, the substitution of (A 37) into (A 38) gives rise to

$$1019 \quad \tilde{J}_{34} = -\tilde{J}_{43} = -\frac{i\pi}{4} \left(3 - \mathcal{B}^2 \mu^2\right) \left(1 + \mathcal{B}^2 \mu^2\right) \frac{\left[\left(\mathcal{N}^2 - \mathcal{B}^2 + 2\right) \mu^2 + \left(1 - \mathcal{N}^2\right)\right]}{\left[\left(\mathcal{N}^2 - 2\mathcal{B}^2 - 4\right) \mu^2 + \left(2 - \mathcal{N}^2\right)\right]}, \quad (\text{A } 38)$$

which is identical to (A 32). The difference is due to the fact that, in (A 32), the parameter  $\mu$   
is described by (3.14), whereas in (A 38) it is given by (3.23). It then results in the expression

$$\frac{\sigma_{ms}}{\varepsilon} = \frac{1}{2\pi} (\operatorname{Re} \alpha)_{max} = \frac{1}{2\pi} \sqrt{\tilde{J}_{34}\tilde{J}_{43}} = \sqrt{-(\tilde{J}_{34})^2} \geq 0$$

1020 given by (3.25) in which the parameter  $\mu$  is given by (3.23).

### 1021 A.3.3. Case 3

1022 The resonance (of order  $n = 2$ ) between a fast mode and a slow mode is characterised by  
1023  $\omega_1 - \omega_3 = 2$ . If this resonant case is destabilising, its maximal growth rate is then of the form

$$1024 \quad \sigma_{mm} = \frac{\varepsilon}{2\pi} (\operatorname{Re} \alpha)_{max} = \frac{\varepsilon}{2\pi} \sqrt{\tilde{J}_{13}\tilde{J}_{31}} \quad (\text{A } 39)$$

1025 where

$$1026 \quad \tilde{J}_{13} = \left(\mathbf{T}^{-1}\right)_{11} (H_{11}^+ T_{13} + H_{14}^+ T_{43}) + \left(\mathbf{T}^{-1}\right)_{12} (H_{21}^+ T_{13} + H_{24}^+ T_{43}) \quad (\text{A } 40a)$$

$$1027 \quad \tilde{J}_{31} = \left(\mathbf{T}^{-1}\right)_{31} (H_{11}^+ T_{11} + H_{14}^+ T_{41}) + \left(\mathbf{T}^{-1}\right)_{32} (H_{21}^+ T_{11} + H_{24}^+ T_{41}) \quad (\text{A } 40b)$$

1029 With the aid of (A 10), (A 11) and (A 27) we find

$$1030 \quad \tilde{J}_{13} = \frac{i\pi(1 - \mu^2)}{8\omega_3(\omega_1^2 - \omega_3^2)} \left(\left(4 - \mathcal{N}^2\right) \omega_3^2 + \mathcal{B}^2 \mathcal{N}^2 \mu^2\right) \left(\omega_1 - \frac{\omega_1 \omega_3^2}{\mathcal{B}^2 \mu^2} + 2\mu^2\right) \quad (\text{A } 41a)$$

$$1031 \quad \tilde{J}_{31} = \frac{i\pi(1 - \mu^2)}{8\omega_1(\omega_3^2 - \omega_1^2)} \left(\left(4 - \mathcal{N}^2\right) \omega_1^2 + \mathcal{B}^2 \mathcal{N}^2 \mu^2\right) \left(\omega_3 - \frac{\omega_3 \omega_1^2}{\mathcal{B}^2 \mu^2} - 2\mu^2\right). \quad (\text{A } 41b)$$

1032

1033 We set

$$1034 \quad \mathcal{A}_0 = -\frac{(1 - \mu^2)}{(\omega_1^2 - \omega_3^2)^2}, \quad (\text{A } 42a)$$

$$1035 \quad \mathcal{A}_1 = \left( (4 - \mathcal{N}^2) \omega_3^2 + \mathcal{B}^2 \mathcal{N}^2 \mu^2 \right) \left( (4 - \mathcal{N}^2) \omega_1^2 + \mathcal{B}^2 \mathcal{N}^2 \mu^2 \right), \quad (\text{A } 42b)$$

$$1036 \quad \mathcal{A}_2 = \frac{(1 - \mu^2)}{\omega_1 \omega_3} \left( \omega_1 - \frac{\omega_1 \omega_3^2}{\mathcal{B}^2 \mu^2} + 2\mu^2 \right) \left( \omega_3 - \frac{\omega_3 \omega_1^2}{\mathcal{B}^2 \mu^2} - 2\mu^2 \right) \quad (\text{A } 42c)$$

1037

so as

$$\tilde{J}_{13} \tilde{J}_{31} = \frac{\pi^2}{64} \mathcal{A}_0 \mathcal{A}_1 \mathcal{A}_2.$$

1038 To calculate the quantities  $\mathcal{A}_0$ ,  $\mathcal{A}_1$  and  $\mathcal{A}_2$  we proceed as follows. We use the resonance  
1039 condition either in the form  $\omega_1 - \omega_3 = 2$  or in an equivalent form (see equation (3.31))

$$1040 \quad 1 - \mu^2 = \frac{16}{(4 - \mathcal{N}^2)^2} \mathcal{B}^2 \mu^2 \quad (\text{A } 43)$$

1041 together with the expressions of  $\omega_1$  and  $\omega_3$  described by (3.3) and determine  $\omega_1 \omega_3$ ,  $\omega_1^2 + \omega_3^2$   
1042 and  $(\omega_1^2 - \omega_3^2)^2$

$$1043 \quad \omega_1 \omega_3 = -\frac{(4 + \mathcal{N}^2)}{(4 - \mathcal{N}^2)} \mathcal{B}^2 \mu^2, \quad (\text{A } 44a)$$

$$1044 \quad \omega_1^2 + \omega_3^2 = 2(2 + \omega_1 \omega_3), \quad (\text{A } 44b)$$

$$1045 \quad (\omega_1^2 - \omega_3^2)^2 = 16(1 + \omega_1 \omega_3) \quad (\text{A } 44c)$$

1046

1047 We therefore substitute (A 44) into (A 42) to obtain

$$1048 \quad \mathcal{A}_0 = -\frac{\mathcal{B}^2}{(4 - \mathcal{N}^2)^2 + \mathcal{B}^2 \mathcal{N}^4} \quad (\text{A } 45a)$$

$$1049 \quad \mathcal{A}_1 = (4 - \mathcal{N}^2)^3 (1 - \mu^2) \left[ (4 - \mathcal{N}^2) (1 - \mu^2) + 4\mathcal{N}^2 \right], \quad (\text{A } 45b)$$

$$1050 \quad \mathcal{A}_2 = -\frac{(1 - \mu^2)}{\mathcal{B}^2 (4 + \mathcal{N}^2)} \left[ (4 - \mathcal{N}^2) (1 - \mu^2) + 4\mathcal{N}^2 \right]. \quad (\text{A } 45c)$$

1051

1052 Thus, we deduce the expression of  $\sigma_{mm}/\varepsilon$  given by (3.32).

1053 **Declaration of interests.** The authors report no conflict of interest.

1054 **Author ORCIDs.** Abdelaziz Salhi <https://orcid.org/0000-0002-3154-345X>.

## REFERENCES

- 1055 Aravind, H. M., Dubos, T., & Mathur, M. 2022 Local stability analysis of homogeneous and stratified  
1056 Kelvin–Helmholtz vortices. *J. Fluid Mech.* **943**, A18.
- 1057 Bajer, K. & Mizerski, K. A. 2013 Elliptical Flow Instability in a Conducting Fluid Triggered by an External  
1058 Magnetic Field. *Phys. Rev. Lett.* **110**, 104503.
- 1059 Balbus, S. A., & Hawley, J. F. 1991 A powerful local shear instability in weakly magnetised disks. I-Linear  
1060 analysis. *Astrophys. J.*, **376**, 214-222.
- 1061 Barker, A. J., & Lithwick, Y. 2013. Non-linear evolution of the tidal elliptical instability in gaseous planets  
1062 and stars. *Mon Not R Astron Soc.*, **435** (4), 3614-3626.

- 1063 Barker, A. J., Braviner, H. J., & Ogilvie, G. I. 2016. Non-linear tides in a homogeneous rotating planet or  
1064 star: global modes and elliptical instability. *Mon Not R Astron Soc.*, **459** (1), 924-938.
- 1065 Barker, A. J. 2016. Non-linear tides in a homogeneous rotating planet or star: global simulations of the  
1066 elliptical instability. *Mon Not R Astron Soc.*, **459** (1), 939-956.
- 1067 Barker, A. J., & Lithwick, Y. 2014 Non-linear evolution of the elliptical instability in the presence of weak  
1068 magnetic fields. *Mon Not R Astron Soc.*, **437** (1), 305-315.
- 1069 Bayly, B. J. 1986 Three-Dimensional instability of elliptical flow. *Phys. Rev. Lett.* **57** (17), 2160-2163.
- 1070 Benkacem, N., Salhi, A., Khlifi, A., Nasraoui, S., & Cambon, C. 2022 Destabilizing resonances of precessing  
1071 inertia-gravity waves. *Phys. Rev. E*, **105** (3), 035107.
- 1072 Cambon, C. 1982 Etude spectrale d'un champ turbulent incompressible, soumis à des effets couplés  
1073 de déformation et de rotation, imposés extérieurement. (Doctoral dissertation, Université Claude  
1074 Bernard-Lyon I).
- 1075 Cambon, C., Teissedre, C., & Jeandel, D. 1985. Etude d'effets couplés de déformation et de rotation sur une  
1076 turbulence homogène. *Journal de mécanique théorique et appliquée*, 4(5), 629-657.
- 1077 Cébron, D., Le Bars, M., Le Gal, P., Moutou, C., Leconte, J., & Sauret, A. 2013. Elliptical instability in hot  
1078 Jupiter systems. *Icarus*, **226** (2), 1642-1653.
- 1079 Chang, C., & Smith, S. G. L. 2021 Density and surface tension effects on vortex stability. Part 2.  
1080 Moore-Saffman-Tsai-Widnall instability. *J. Fluid Mech.*, **913** A15.
- 1081 Chandrasekhar, S. 1961 *Hydrodynamic and hydromagnetic stability*. Clarendon Press.
- 1082 Chagelishvili, G. D., Zahn, J. P., Tevzadze, A. G., & Lominadze, J. G., 2003 On hydrodynamic shear  
1083 turbulence in Keplerian discs: via transient growth to bypass transition. *A & A* **402**, 401-407.
- 1084 Craik, A. D. D. & Criminale, W. O. 1986 Evolution of wave-like disturbances in shear flows. A class of  
1085 exact-solutions of the Navier-Stokes equations. *Proc. R. Soc. Lond. A* **406**, 13-26.
- 1086 Craik, A. D. D. 1989 The stability of unbounded two- and three-dimensional flows subject to body forces:  
1087 some exact solutions. *J. Fluid Mech.* **198**, 275-292.
- 1088 Crow, S. C. 1970 Stability theory for a pair of trailing vortices. *AIAA journal*, **8** (12), 2172-2179.
- 1089 Davidson, P. A. 2013 *Turbulence in rotating, stratified and electrically conducting fluids*. Cambridge  
1090 University Press.
- 1091 Éloy, C., & Le Dizès, S. 2001 Stability of the Rankine vortex in a multipolar strain field. *Phys. Fluids*, **13**  
1092 (3), 660-676.
- 1093 Feys, J., & Maslowe, S. A. 2016 Elliptical instability of the Moore-Saffman model for a trailing wingtip  
1094 vortex. *J. Fluid Mech.*, **803**, 556-590.
- 1095 Fukumoto, Y. 2003 The three-dimensional instability of a strained vortex tube revisited. *J. Fluid Mech.*, **493**,  
1096 287-318.
- 1097 Gledzer, E. B., Dolzhansky, F. V., Obukhov A. M., Ponomarev V. M. 1975 An experimental and theoretical  
1098 study of the stability of a liquid in an elliptical cylinder. *Isv. Atmos. Ocean. Phys.* **11**:617-22.
- 1099 Godeferd, F. S., Cambon, C., & Leblanc, S. 2001 Zonal approach to centrifugal, elliptic and hyperbolic  
1100 instabilities in Stuart vortices with external rotation. *J. Fluid Mech.*, **449**, 1-37.
- 1101 Guimbard, D., Le Dizès, S., Le Bars, M., Le Gal, P., & Leblanc, S. 2010 Elliptic instability of a stratified  
1102 fluid in a rotating cylinder. *J. Fluid Mech.*, **660**, 240-257.
- 1103 Kelvin, L. (1887). Stability of fluid motion: rectilinear motion of viscous fluid between two parallel plates.  
1104 *Phil. Mag.* **24** (5), 188-196.
- 1105 Herreman, W., Cébron, D., Le Dizès, S., & Le Gal, P. 2010 Elliptical instability in rotating cylinders: liquid  
1106 metal experiments under imposed magnetic field. *J. Fluid Mech.*, **661**, 130-158.
- 1107 Kerswell, R. R. 1993a. The instability of precessing flow. *Geophys. Astrophys. Fluid Dyn.* **72** (1-4), 107-144.
- 1108 Kerswell, R. R. 1993b Elliptical instabilities of stratified, hydromagnetic waves. *Geophys. Astrophys. Fluid*  
1109 *Dyn.* **71** (1-4), 105-143.
- 1110 Kerswell, R. R. 1994 Tidal excitation of hydromagnetic waves and their damping in the Earth. *J. Fluid*  
1111 *Mech.*, **274**, 219-241.
- 1112 Kerswell, R. R. 2002 Elliptical instability. *Annu. Rev. Fluid Mech.* **34**, 83-113.
- 1113 Kuchment, P. A. 1993 *Floquet theory for partial differential equations* (Vol. **60**). Springer Science &  
1114 Business Media.
- 1115 Landman, M. J. & Saffman, P. G. 1987 The three-dimensional instability of strained vortices in a viscous  
1116 fluid. *Phys. Fluids* **30** (8), 2339-2342.
- 1117 Le Bars, M. & Le Dizès, S. 2006 Thermo-elliptical instability in a rotating cylindrical shell. *J. Fluid. Mech.*  
1118 **563**, 189-198.

- 1119 Lebovitz, N. R. & Zweibel, E. 2004 Magnetoelliptic instabilities. *Astrophys. J.* **609**, 301–312.
- 1120 Le Reun, T., Favier, B., & Le Bars, M. 2019 Experimental study of the nonlinear saturation of the elliptical  
1121 instability: inertial wave turbulence versus geostrophic turbulence. *J. Fluid Mech.*, **879**, 296–326.
- 1122 Lesur, G. & Papaloizou, J. C. B. 2009 On the stability of elliptical vortices in accretion discs. *Astron.*  
1123 *Astrophys.* **498**, 1–12.
- 1124 Leweke, T., Le Dizes, S., & Williamson, C. H. 2016 Dynamics and instabilities of vortex pairs. *Annu. Rev.*  
1125 *Fluid Mech.*, **48**, 507–541.
- 1126 Lifschitz, A., & Hameiri, E. 1991 Local stability conditions in fluid dynamics. *Phys. Fluids A*: **3** (11),  
1127 2644–2651.
- 1128 Lifschitz A. 1994 On the stability of certain motions of an ideal incompressible fluid. *Adv. Appl. Math.*  
1129 **15**:404–36.
- 1130 Malkus, W. V. R. 1989 An experimental study of the global instabilities due to the tidal (ellip- tical) distortion  
1131 of a rotating elastic cylinder. *Geophys. Astrophys. Fluid Dyn.* **48**:123– 34.
- 1132 McKeown, R., Ostilla-Mónico, R., Pumir, A., Brenner, M. P., & Rubinstein, S. M. 2020 Turbulence  
1133 generation through an iterative cascade of the elliptical instability. *Science advances*, **6** (9), eaaz2717.
- 1134 Mizerski, K. A. & Bajer, K. 2009 The magnetoelliptic instability of rotating systems. *J. Fluid Mech.* **632**  
1135 (1), 401–430.
- 1136 Mizerski, K. A., & Lyra, W. 2012 On the connection between the magneto-elliptic and magneto-rotational  
1137 instabilities. *J. Fluid Mech.*, **698**, 358–373.
- 1138 Miyazaki, T. 1993 Elliptical instability in a stably stratified rotating fluid. *Phys. Fluids A* **5** (11), 2702–2709.
- 1139 Miyazaki, T. & Fukumoto, Y. 1992 Three-dimensional instability of strained vortices in a stably stratified  
1140 fluid. *Phys. Fluids A* **4** (11), 2515–2522.
- 1141 Moffatt, H. K. 2010. Note on the suppression of transient shear-flow instability by a spanwise magnetic field.  
1142 *J. Eng. Math.* **68**, 263–268.
- 1143 Moore, D.W. & Saffman, P.G. 1975 The instability of a straight vortex filament in a strain field. *Proc. R.*  
1144 *Soc. Lond. A* **346**, 413–425.
- 1145 Nornberg, M. D., Ji, H., Schartman, E., Roach, A., & Goodman, J. 2010 Observation of magnetocoriolis  
1146 waves in a liquid metal Taylor-Couette experiment. *Phys. Rev. Lett.*, **104** (7), 074501.
- 1147 Ogilvie, G. I. 2014 Tidal dissipation in stars and giant planets. *Annu. Rev. Astron. Astrophys.*, **52**, 171–210.
- 1148 Otheguy, P., Chomaz, J. M., & Billant, P. 2006 Elliptic and zigzag instabilities on co-rotating vertical vortices  
1149 in a stratified fluid. *J. Fluid Mech.*, **553**, 253–272.
- 1150 J. Pedlosky, J. 2013 *Geophysical Fluid Dynamics*. Springer Science & Business Media, Berlin.
- 1151 Pierrehumbert, R. T. 1986 Universal short-wave instability of two-dimensional eddies in an inviscid fluid.  
1152 *Phys. Rev. Lett.* **57** (17), 2157–2159.
- 1153 Sagaut, P., & Cambon, C. 2008 *Homogeneous turbulence dynamics*. First Edition, CUP Cambridge 2008,  
1154 Second Edition, Springer Cham, 2018.
- 1155 Schecter, D. A., Boyd, J. F., & Gilman, P. A. 2001 “Shallow-water” magnetohydrodynamic waves in the  
1156 Solar tachocline. *Astrophys. J.*, **551** (2), L185.
- 1157 Salhi, A., & Cambon, C. 1997 An analysis of rotating shear flow using linear theory and DNS and LES  
1158 results. *J. Fluid Mech.*, **347**, 171–195.
- 1159 Salhi, A., & Cambon, C. 2009 Precessing rotating flows with additional shear: Stability analysis. *Phys. Rev.*  
1160 *E*, 79(3), 036303.
- 1161 Salhi, A., Lehner, T., & Cambon, C. 2010 Magnetohydrodynamic instabilities in rotating and precessing  
1162 sheared flows: An asymptotic analysis. *Phys. Rev. E*, **82** (1), 016315.
- 1163 Salhi, A., Lehner, T., Godeferd, F., & Cambon, C. 2012 Magnetized stratified rotating shear waves. *Phys.*  
1164 *Rev. E*, **85** (2), 026301.
- 1165 Salhi, A., Baklouti, F. S., Godeferd, F., Lehner, T., & Cambon, C. 2017 Energy partition, scale by scale, in  
1166 magnetic Archimedes Coriolis weak wave turbulence. *Phys. Rev. E*, **95** (2), 023112.
- 1167 Salhi, A., Khlifi, A., & Cambon, C. 2020. Nonlinear effects on the precessional instability in magnetised  
1168 turbulence. *Atmosphere*, **11**(1), 14.
- 1169 Singh, S., & Mathur, M. 2019 Effects of Schmidt number on the short-wavelength instabilities in stratified  
1170 vortices. *J. Fluid Mech.*, **867**, 765–803.
- 1171 Sipp, D., Lauga, E., & Jacquin, L. 1999. Vortices in rotating systems: centrifugal, elliptic and hyperbolic  
1172 type instabilities. *Phys. Fluids*, **11** (12), 3716–3728.
- 1173 Sipp, D. & Jacquin, L. 2003 Widnall instabilities in vortex pairs. *Phys. Fluids* **15**, 1861–1874..

- 1174 Slane, J., & Tragesser, S. 2011 Analysis of periodic nonautonomous inhomogeneous systems. *Nonlinear*  
1175 *Dyn. Syst. Theory*, **11** (2), 183-198.
- 1176 Suzuki, S., Hirota, M., & Hattori, Y. 2018 Strato-hyperbolic instability: a new mechanism of instability in  
1177 stably stratified vortices. *J. Fluid Mech.*, **854**, 293-323.
- 1178 Tsai, C. Y., & Widnall, S. E. 1976 The stability of short waves on a straight vortex filament in a weak  
1179 externally imposed strain field. *J. Fluid Mech.*, **73** (4), 721-733.
- 1180 Waleffe, F. 1989 The 3 – *D* instability of a strained vortex and its relation to turbulence (Doctoral dissertation,  
1181 *PhD thesis* MT).
- 1182 Waleffe, F. 1990 On the three-dimensional instability of strained vortices. *Phys. Fluids A* **2** (1), 76–80.
- 1183 Waleffe, F. 1992 The nature of triad interactions in homogeneous turbulence. *Phys. Fluids A*, **4**(2), 350-363.
- 1184 Wang, Y., Gilson, E. P., Ebrahimi, F., Goodman, J., & Ji, H. 2022 Observation of axisymmetric standard  
1185 magnetorotational instability in the laboratory. *Phys. Rev. Lett.*, **129** (11), 115001.
- 1186 Wilczyński, F., Hughes, D. W., & Kersalé, E. 2022. Magnetic buoyancy instability and the anelastic  
1187 approximation: regime of validity and relationship with compressible and Boussinesq descriptions.  
1188 *J. Fluid Mech.*, **942**, A46.
- 1189 Zwirner, L., Tilgner, A., & Shishkina, O. 2020 Elliptical instability and multiple-roll flow modes of the  
1190 large-scale circulation in confined turbulent Rayleigh-Bénard convection. *Phys. Rev. Lett.*, **125** (5),  
1191 054502.